CHALMERS
UNIVERSITY OF TECHNOLOGY

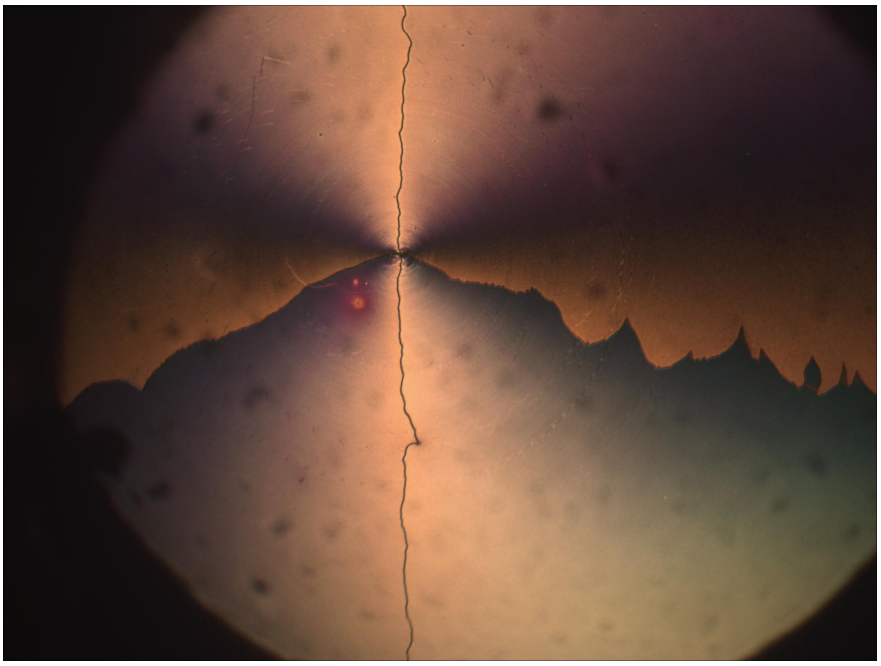

Alignment of a Ferroelectric Nematic Liquid Crystal on Surfaces Treated with Obliquely Evaporated SiO_2

Master's thesis in Nanotechnology

EBBA GRÖNFORS

DEPARTMENT OF MICROTECHNOLOGY AND NANOSCIENCE
CHALMERS UNIVERSITY OF TECHNOLOGY
Gothenburg, Sweden 2023
www.chalmers.se

Master's thesis 2023

Alignment of a Ferroelectric Nematic Liquid Crystal on Surfaces Treated with Obliquely Evaporated SiO_2

EBBA GRÖNFORS

CHALMERS
UNIVERSITY OF TECHNOLOGY

Department of Microtechnology and Nanoscience
Division of Electronics Materials and Systems
Chalmers University of Technology
Gothenburg, Sweden 2023

Alignment of a Ferroelectric Nematic Liquid Crystal on Surfaces Treated with Obliquely Evaporated SiO_2
EBBA GRÖNFORS

Supervisor: Per Rudquist
Examiner: Per Rudquist

Master's Thesis 2023
Department of Microtechnology and Nanoscience
Division of Electronics Materials and Systems
Chalmers University of Technology
SE-412 96 Gothenburg
Telephone +46 31 772 1000

Cover: An evaporated CRC with $\alpha = 30°$ between crossed polarizers, with evaporation direction from left to right. The cell contains RM734 in the N phase, and the temperature is 150°C.

Typeset in LaTeX
Printed by Chalmers Reproservice
Gothenburg, Sweden 2023

Alignment of a ferroelectric nematic liquid crystal on surfaces treated with obliquely evaporated SiO_2

EBBA GRÖNFORS
Department of Microtechnology and Nanoscience
Chalmers University of Technology

Abstract

A nematic liquid crystal is an orientationally ordered liquid where molecules align along a local director but with no polar order. The material RM734 is one of very few discovered substances that can assume the ferroelectric nematic phase, a liquid crystal phase first practically realized in 2017 where the director has not only an orientation, but also a direction. This thesis qualitatively describes the alignment of RM734 in the nematic and ferroelectric nematic phase on a surface treated with oblique evaporation of SiO_2. The alignment is studied by means of a thin cell where one surface has been treated with oblique evaporation of SiO_2 and the opposite surface is covered by a polymer which has been rubbed to achieve circular boundary conditions. The alignment is revealed by the formation and behavior of domains, depending on the local mutual alignment directions on the two surfaces. The domains created in the higher symmetry nematic phase has a large impact on the alignment in the ferroelectric nematic phase. It is found that the material aligns at an azimuthal angle $0° < \phi < 90°$ from the evaporation plane in either of two symmetrical directions approximately in the substrate plane, potentially opening up for the design of devices based on bistable alignment. The angle ϕ depends on both temperature and evaporation angle, and turns out to fixate under certain conditions. This adds a new layer of complexity to the alignment, as time becomes an important factor in its behavior. RM734 is also studied in a cell with parallel non-polar boundary conditions. Using this cell, the behavior of the liquid crystal at the transitions between the nematic and ferroelectric nematic phases is mapped, and a spontaneous twist without a preferred handedness is demonstrated in the ferroelectric nematic phase.

Keywords: liquid crystal, ferroelectric nematic phase, nematic phase, oblique evaporation, alignment, liquid crystal alignment, surface anchoring, cleanroom fabrication, myfab

Acknowledgements

Thank you to my supervisor Per Rudquist for all the guidance, support and enthusiasm throughout the project. I also want to thank the Liquid Crystal Physics group at the University of Colorado at Boulder for their invaluable response on my lab results. This work was performed in part at Myfab Chalmers. A first batch of RM734 was kindly provided by Eva Korblova and David M. Walba at the University of Colorado at Boulder, and a second batch was provided through the University of Stuttgart. Lastly, thank you to Henrik Frederiksen for the guidance in the cleanroom and to Mats Myremark for fixing broken equipment.

Ebba Grönfors, Gothenburg, June 2023

List of Acronyms

Below is the list of acronyms that have been used throughout this thesis listed in alphabetical order:

BC	Boundary Condition
CRC	Circularly Rubbed Cell
DEC	Double Evaporated Cell
ECRC	Evaporated Circularly Rubbed Cell
ITO	Indium Tin Oxide
LC	Liquid Crystal
N	Nematic Phase
N_F	Ferroelectric Nematic Phase
N_S	Splay Nematic Phase
PI	Polyimide
POM	Polarized Optical Microscopy
QDR	Quick Dump Rinse
SC1	Standard Clean 1
SmA	Smectic A
TN	Twisted Nematic

Contents

List of Figures

1

Introduction

Liquid crystals are a collection of different states of matter beyond the well known solid, liquid and gas phases. They consist of molecules which flow freely like a liquid while also forming a crystal-like pattern, breaking some symmetry by introducing a level of order. This combination of liquid-like and crystal-like properties make them useful in many technological fields.

The simplest liquid crystal phase is the nematic phase, where the molecular axes align with a local director. This orientational order can be controlled by external factors such as patterned surfaces or electric fields. The most well known application of the nematic liquid crystal is in liquid crystal displays. Their interaction with polarized light is the key to constructing pixels that can switch between being dark and bright by applying an electric field.

In 2017, the new material RM734 was synthesized by Mandle et al [1][2]. This material is the first liquid crystal material identified to exhibit the ferroelectric nematic phase, and has become the standard material used for studying it. Previously, this phase has only been studied theoretically. The ferroelectric nematic phase is similar to the nematic phase, but also has a polarity which could open up possibilities for new technological applications in the future. At this point in time the phase is still investigated in fundamental research, as a century of theoretical knowledge regarding the phase is being evaluated experimentally for the first time.

1.1 Aim

The aim of this thesis is to describe the alignment of the liquid crystal material RM734 in the nematic and ferroelectric nematic phases on a surface treated with oblique evaporation of SiO_2. This is done by creating glass cells with known boundary conditions, and studying these cells filled with RM734 using polarization microscopy. Previous studies have investigated the alignment of RM734 on different surfaces [3][4][5], as well as the alignment of other nematic liquid crystals on surfaces similar to the one centered on in this report [6][7]. However, the alignment of a material able to enter the ferroelectric nematic phase on obliquely evaporated surface layers has not been reported before.

1.2 Problem definition

The objective in this project can be summarized with the following questions:

- How does RM734 in the nematic phase align on a surface treated with oblique evaporation of SiO_2?
- How does the ferroelectric nematic phase align on a surface treated with oblique evaporation of SiO_2, and how does it differ from the nematic phase?
- What happens at the transition between the two cases mentioned above?
- Can the interaction between the ferroelectric nematic phase and a surface treated with oblique evaporation of SiO_2 be made to be polar or non-polar through the choice of evaporation parameters?

1.3 Limitations

The questions above cover a wide scope, and some limitations have been necessary. The main focus of this project has been the alignment in a certain type of cell, called an evaporated circularly rubbed cell, which is described further in section 3.1.3.1, and the results do not necessarily reflect the alignment in an arbitrary geometry. The alignment of RM734 in the studied cells is described in mostly qualitative terms and a number of factors which affect the alignment are identified. The thesis provides a first overlook of the factors, and thus more detailed and quantitative investigation of them is left for future research.

2

Theory

2.1 What is a Liquid Crystal?

A liquid crystal (LC) consists of non-spherical molecules which tend to align in a common direction. What makes an LC special is that it has a higher order than a liquid, which has neither positional nor orientational long-range order, but lower order than a crystal, which has both three-dimensional long-range positional and orientational order. An LC has directional order and sometimes some degree of positional order in one or multiple directions. Three different phases with different types of order can be seen in Figure 2.1.

In its simplest form, the LC is built up of rod-like molecules. This is called a calamitic LC. One can imagine these as a large number of matchsticks in a box. The matchsticks take up significantly less space if they all align in the same direction, so that configuration will minimize the energy of the matchsticks. In the case of a real thermotropic LC, there are also attractive intermolecular forces stabilising the phase, and, depending on the phase, other types of order may appear. Some LCs also consist of for example disk-like or banana-shaped molecules.

LCs can be divided into two groups; Thermotropic LCs, where the phase of a sample is mainly determined by its temperature, and lyotropic LCs, where it is mainly determined by its concentration. This project focuses on a thermotropic LC, RM734, which is described in detail in section 2.4.1. [8]

(a) Isotropic **(b)** Nematic (N) **(c)** Smectic A (SmA)

Figure 2.1: Three different phases built up of rod-like molecules with different types of order. In the isotropic phase, there is no positional or orientational order. In the N and SmA phases, there is orientational order, as the molecules are approximately vertically oriented. The SmA phase also has some positional order, as the molecules are positioned in layers.

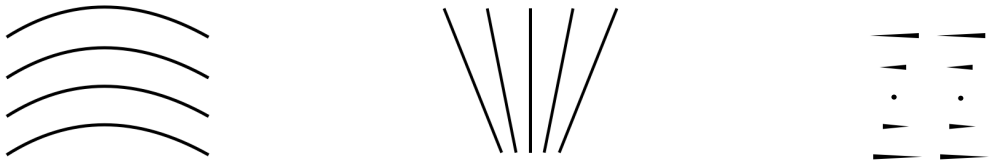

(a) Bend **(b)** Splay **(c)** Twist

Figure 2.2: The director field, represented as black lines, with the three elementary types of deformations. For tapered lines, the thin ends point into the page. Bend and splay are shown in the 2-dimensional case, while the twist case twists out of the page.

2.1.1 The Director

The director, $\hat{\mathbf{n}}$, is a unit vector used to describe the orientational field of an LC. It corresponds to the local average direction of the molecular axes.

The vast majority of LCs have a non-polar symmetry, where $\hat{\mathbf{n}} = -\hat{\mathbf{n}}$. That means the preferred direction of the molecules is either of two opposite directions. This is the main difference between the director field and other vector fields such as magnetic fields. [8]

2.1.2 Deformations

The director field does not have to be constant in the bulk of an LC, but can vary gradually across space. These variations can be described in terms of bend, splay and twist, all seen in Figure 2.2. Multiple of these types of deformations can also coexist in an LC, leading to more complex director fields. They can be induced by the surrounding boundary conditions, or by the shape of or interactions between the LC molecules.

Nematic LCs have an orientational elasticity, which means that the different types of curvature deformations in Figure 2.2 give rise to a deformation elastic energy density. Deformations generally increase the energy of the system, and the amount of energy required are different for each type of deformation. For some LCs, the most relaxed possible state naturally has a certain amount of bend, twist or splay. For example, if the LC is doped with a chiral material the state with the lowest energy will have some twist, and deviations from this relaxed states increases the elastic energy in the system. [8]

2.1.3 Disclinations

Disclinations in an LC are places where the director is undefined. These places could be points or lines. What they have in common is that the orientation of $\hat{\mathbf{n}}$ changes discontinuously when passing through the disclination.

The strength of a line disclination is defined as the number of whole rota-

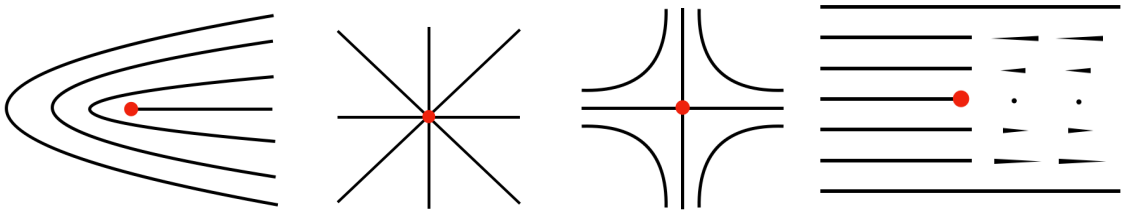

(a) $s = +1/2$ **(b)** $s = +1$ **(c)** $s = -1$ **(d)** Möbius, $|s| = 1/2$

Figure 2.3: Cross section of director fields around line disclinations with different strengths. The black lines represent the director, and the red spots mark disclinations. All images show the 2-dimensional case of the different types of disclination, with the exception of the Möbius disclination which is 3-dimensional.

tions of the director in positive mathematical direction when going around the disclination in the same direction. Examples of disclinations of the strengths $+1/2$, $+1$ and -1 can be seen in Figure 2.3. In three dimensions the director may also rotate in any plane parallel to the line disclination when going around it, forming a Möbius disclination. In those cases, the absolute value of the strength of the disclination can be calculated in the same way as when $\hat{\mathbf{n}}$ rotates in the cross section plane, but the sign of the strength can not be defined since it would depend on the angle from which the system is viewed. [8]

In this project, line disclinations between different domains are of big importance. Specifically, domains with a twist of opposite handedness from each other will be separated with a Möbius disclination, as there is no way for the director to continuously change from a twist with one handedness to the other while conforming to the surrounding BCs.

2.1.4 The Nematic Phase

The simplest LC phase is the nematic (N) phase, seen in Figure 2.1b, where the only type of order is orientational order. In this phase $\hat{\mathbf{n}}$ simply aligns with one orientation, leading to a cylindrically symmetric structure. This is the phase commonly used in displays, as it is easy to align in a way that creates a smooth texture. Like in most known LC phases, $\hat{\mathbf{n}} = -\hat{\mathbf{n}}$ is true for N, giving it non-polar symmetry. [8]

The material E7, which is a well-studied standard mixture of four different LCs, is in the N phase at room temperature and transitions into the isotropic phase at about 60°C. This makes it convenient for studying the N phase, since it does not necessarily require a hot stage or any other way to keep it at a high temperature throughout an experiment. In this study, E7 will be used as a reference in order to compare the results to earlier observations.

2.2 Studying LCs

An effect of the orientational order in an LC is that it gives rise to a birefringence. Birefringence means that light that passes through the LC is refracted differently depending on its polarization. This can be taken advantage of in order to study LCs using polarized light. [9]

In order to create a controlled environment for an LC to be studied in, thin glass cells can be used. The cell gap is typically a few μm, which is thin enough to in combination with LC elasticity define the quiescient state in the cell.

2.2.1 Polarized Optical Microscopy

The method used in this project to study LCs is polarized optical microscopy (POM). In POM, a cell containing an LC is placed under a microscope between two polarization filters, and a beam of light passes through the sample. The microscope magnifies the image such that any disclinations are made visible. The sample can be rotated and the polarizers can be crossed and de-crossed to investigate different properties of the LC. [8]

The change in polarization when light passes through a birefringent material depends on its wavelength, the thickness of the LC and the effective optical anisotropy. Therefore, when white light is used in POM not all wavelengths will pass through the sample, and the result will be an image in a certain colour. If the thickness of the cell is known, a Michel-Levy chart can be used to deduct the birefringence of the sample based on the colour. [10]

2.2.2 Boundary Conditions

To create specific known director fields to study, boundary conditions (BCs) can be applied to the LC. This means that in addition to confining it in a thin glass cell, the direction of $\hat{\mathbf{n}}$ is controlled through different treatments of the surfaces of the cell. The simplest form of BCs is rubbing the glass with a velvet roll. This makes the LC align along the rubbing direction. If the rubbing is parallel on both surfaces this leads to large homogeneous domains within the cell. Non-parallel rubbing can be used to study different amounts of twist in $\hat{\mathbf{n}}$. [11]

A different method to create BCs is oblique evaporation. The method was patented in 1979 by Janning, and consists of evaporating an inorganic material onto a tilted substrate. In this thesis, SiO_2 is used. The oblique evaporation creates different BCs depending on the evaporation angle, α, defined as the angle between the substrate normal and the direction of the incoming particles, as shown in Figure 2.4. The direction of the incoming particles will be referred to as the evaporation direction, and the plane spanned by the evaporation direction and its projection on the substrate will be referred to as the evaporation plane. [12]

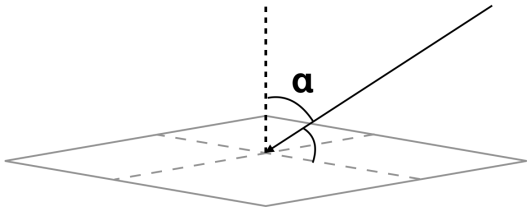

Figure 2.4: The evaporation angle α is defined as the angle between the substrate and the incoming flow of evaporated particles.

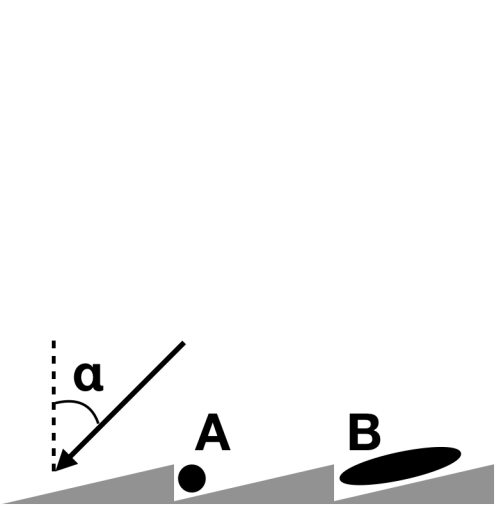

(a) Positions A and B in the evaporation plane

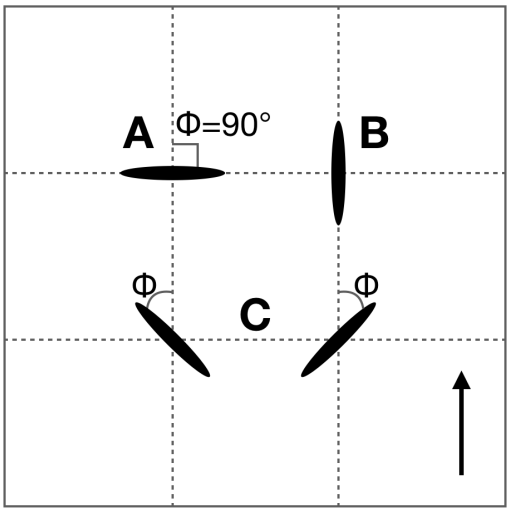

(b) Positions A, B and C in the substrate plane.

Figure 2.5: The different possible directions of $\hat{\mathbf{n}}$ on a substrate treated with oblique evaporation. Position A generally appears when α is small, position B when α is large, and positions C between these two options. The black arrows show the evaporation direction. When viewed from the side, the approximated texture of the surface after oblique evaporation is shown as gray slopes.

The alignment of N on a surface treated with oblique evaporation was studied in depth in 1996 by Jägemalm [6][7]. For small evaporation angles, α, LCs tend to align normal to the evaporation plane, which is spanned by the substrate normal and the direction of the incoming particles, shown by case A in Figure 2.5. For large values of α, LCs tend to align in the evaporation plane, shown by case B in Figure 2.5. The alignment is described by the variable ϕ, which is defined as the angle between the director and the evaporation plane. The angle ϕ is approximately 0° for large α and 90° for small α. In a medium range, two symmetrically positioned states will arise where $0° < \phi < 90°$, shown by cases C in Figure 2.5. In this case, ϕ is generally temperature dependent and varies between 90° at high temperatures and some lower limit ϕ_α at lower temperatures. [6][7]

2.3 Compensators

When a cell is studied between crossed polarizers, one can determine whether or not $\hat{\mathbf{n}}$ is parallel to one of the polarizers, but there is no way to see which one. In some cases the orientation can be determined based on the BCs, but that does not always work unless the BCs and their effect on $\hat{\mathbf{n}}$ is well known. This problem can be solved by using a compensator.

A compensator is a crystal, often quartz, with a known birefringence. This can be added on top of a LC cell between the polarizers. Depending on the orientation of $\hat{\mathbf{n}}$ and the compensator, this will either increase the total birefringence or cancel part of it. If the birefringence of the compensator is the same as that of the LC and they are placed at a 90° angle, they will cancel out completely and there will be light extinction. [13]

2.3.1 Nematic Cells in POM

An LC in the N phase, when placed in a cell with parallel BCs on the top and bottom glass and studied using POM with crossed polarizers, typically gives a homogeneous image in one colour. The largest amount of light is let through when $\hat{\mathbf{n}}$ is at a 45° angle compared to the polarizers. If $\hat{\mathbf{n}}$ is parallel to one of the polarizers, no light will go through and the image will be dark. In the case of parallel polarizers, all light that is blocked with crossed polarizers will instead go through. That means that the image will be white when $\hat{\mathbf{n}}$ is parallel to or at a right angle to the polarizers, and when $\hat{\mathbf{n}}$ is at a 45° angle the colour shown will be the complement to that of the case with crossed polarizers.

When the BCs on the surfaces of a cell provide no preferred orientational order, $\hat{\mathbf{n}}$ changes gradually across the sample. The texture formed is called a schlieren texture, seen in Figure 2.6. The change of $\hat{\mathbf{n}}$ is generally smooth, with the exception of line disclinations spanning from one surface to the other or point disclinations on either of the surfaces. These disclinations appear as points in the image. Each disclination has a number of dark arms, in the directions where $\hat{\mathbf{n}}$ is parallel to one of the polarizers. The number of arms is equal to $4s$, where s is the strength of the disclination. To figure out if the order is positive or negative the sample can be rotated. If the dark arms stay in the same direction as they originally were, the disclination order is positive. If the disclination order is negative, the arms will rotate in the same direction as the sample at twice the speed. The number of arms will always be even, where each pair of arms represents a 180° rotation of $\hat{\mathbf{n}}$. [8]

If BCs are applied to both sides of a cell at a right angle to each other, $\hat{\mathbf{n}}$ will twist gradually across the cell gap in the N phase. This is called Twisted Nematic (TN). When a TN cell is studied between crossed polarizers, it can be rotated without achieving complete light extinction at any angle. When the surface alignments caused by the BCs are parallel to the two polarizers, white light will pass through the sample. At a 45° rotation of the sample the image will show a colour instead

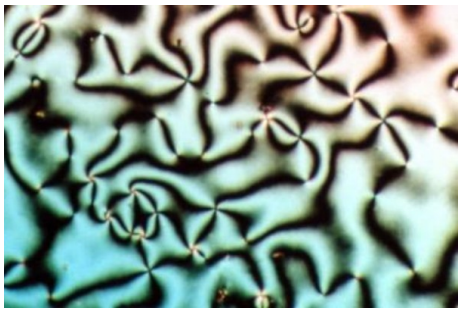

Figure 2.6: Schlieren texture of a N LC viewed using POM. Image from Wikipedia user Minutemen, used under Creative Commons (`https://creativecommons.org/licenses/by-sa/3.0/deed.en`).

of white light. In some cases, LCs can twist more than is necessary to satisfy the BCs, forming a so called supertwist, and this will affect the colours in an image. A supertwist happens if the material naturally twists in its relaxed state, as described in Section 2.1.2. The more $\hat{\mathbf{n}}$ twists across a cell gap, the less the image in POM will be affected by rotation of the sample.

Generally, a TN cell will be divided into different domains where the twist is either lefthanded or righthanded, which may cause problems in many applications since the cell will not appear smooth. There are multiple methods to avoid this. One way is to apply a pre-tilt to the BCs, something that happens naturally when treating the surface through rubbing. The BCs could also be put at a $\sim 85°$ angle from each other instead of a right angle, or the LC could be doped with a chiral material. Each of these methods will lead to one handedness of the twist requiring less energy than the other, and thus being more likely to take place. TN cells are used in certain types of displays, where the N LC is placed between crossed polarizers and the twist changes the polarity of the light passing through it to make a pixel bright. The pixel can be made dark by applying an electric field normal to the cell, making $\hat{\mathbf{n}}$ align with the field instead of forming a twist. [14]

2.4 The Ferroelectric Nematic Phase

The LC phase which is studied in this project is the Ferroelectric Nematic phase (N_F). This phase is closely related to the N phase, which is described above. The main difference is that the N_F phase is a *polar phase*, which means that $\hat{\mathbf{n}} \neq -\hat{\mathbf{n}}$. Therefore, disclinations with non-integer strengths are forbidden since $\hat{\mathbf{n}}$ must rotate 360° to return to its original state rather than just 180°. It also means that two domains with $\hat{\mathbf{n}}$ pointing along the same axis can still have a clear boundary between them due to $\hat{\mathbf{n}}$ pointing in different directions in the two domains. [15]

A theory about the N_F phase was presented by Born in 1916 [16], but it was not until a century later that Mandle et al presented a material which had a N_F phase [1][2]. The phase is also discussed in some literature as the Splay Nematic phase (N_S) since it might be related to spontaneous splay deformations and a low

splay elastic constant. [17]

According to a prediction by Kachaturyan from 1975 [18], a polar phase is expected to have a spontaneous twist due to electrostatic forces. This twist is not arising from chirality in the medium, and will therefore not have a preferred handedness. This affects the expected behavior of $\hat{\mathbf{n}}$, as it may not be homogeneous in a cell where the surrounding BCs are parallel.

2.4.1 RM734

The material RM734 is a rod-like polar molecule, which can assume the N_F phase. The material is crystalline at room temperature, so in order to study the N_F phase it has to be heated up. Its phase sequence is N_F 133°C N 188°C isotropic, where the given temperatures are the transition temperatures between the three phases. [5]

Since RM734 is the first reported LC material that assumes the N_F phase, it has become the standard material for studying the phase. For this reason it has also been chosen as the main LC to be studied in this thesis, so that the results can easily be compared to both previous and future studies.

2.4.2 Polar and Non-Polar BCs

BCs on the surfaces of a cell can be divided into two groups: Polar and non-polar. For the N phase, these two groups behave in approximately the same way. In the N_F phase, however, their behavior differs due to the polarity of the phase. In this case, a polar BC will make one direction of $\hat{\mathbf{n}}$ more energetically favorable than the other.

Rubbing is a polar treatment, since the substrate is always rubbed in a certain direction. In the N phase, $\hat{\mathbf{n}}$ will simply align with the rubbing direction, but in the N_F phase it will specifically align in the same direction as the rubbing has been applied as opposed to aligning against it. In the case of parallel rubbing, this leads to a large domain where $\hat{\mathbf{n}}$ points in the same direction with no disclinations. If the rubbing is anti-parallel, twisted fields with different handedness will appear with a Möbius diclination separating them. [3][4]

Oblique evaporation can theoretically lead to both polar and non-polar BCs depending on the evaporation angle, α [6][7]. The different expected alignments of LCs are shown in Figure 2.7. When α is small, case A in Figure 2.7, $\hat{\mathbf{n}}$ is expected to align in two opposite directions with no difference in energy, due to the symmetry of the substrate. Since the medium is still polar, domains with opposite polarization will form unless one is favoured over the other by the BCs of the opposite surface of the cell and the elasticity of the LC. For medium evaporation angles, $\hat{\mathbf{n}}$ is expected to be bistable at an angle $0° < \phi < 90°$, cases C in Figure 2.7. In these cases, some polarity is expected as the substrate is not symmetrical along the director. Like in case A, the two cases will appear in different domains,

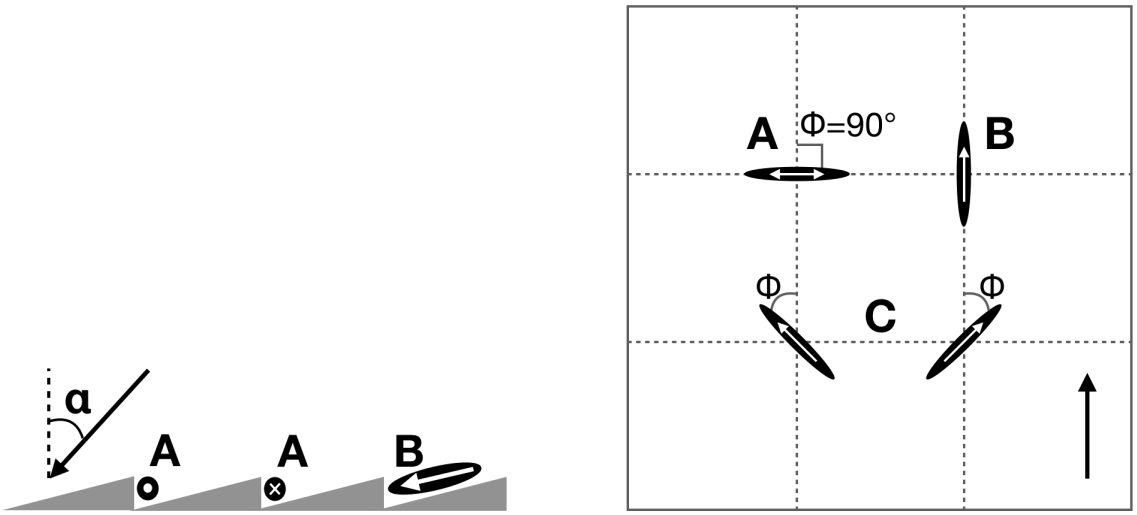

(a) Positions A and B in the evaporation plane

(b) Positions A, B and C in the substrate plane.

Figure 2.7: The different possible directions of $\hat{\mathbf{n}}$ for N_F on a substrate treated with oblique evaporation. Position A appears when α is small, position B when α is large, and positions C between these two options. The black arrows show the evaporation direction. When viewed from the side, the approximated texture of the surface after oblique evaporation is shown as gray slopes.

unless other factors give one of them lower energy. If α is large, $\hat{\mathbf{n}}$ will align according to case B in Figure 2.7, in which case the polarity of the BC will cause $\hat{\mathbf{n}}$ to point in the same direction across the whole cell, making it similar to a rubbed BC.

There is no inherent property saying which direction along $\hat{\mathbf{n}}$ is positive or negative in N_F. In this work, the positive direction is defined to be that pointing along the evaporation direction when aligning at a polar evaporated surface.

2.4.3 Circularly Rubbed Cells

A recent study by Rudquist [5] presented a method to verify that a liquid crystal is in an N_F phase by placing it in a Circularly Rubbed Cell (CRC). The cell consisted of two plates on top of each other, where the bottom plate had been rubbed linearly and the top plate rubbed circularly to create boundary conditions for the alignment of the LC, as shown in Figure 2.8. The simple geometry made it possible to predict the number of disclination lines and their positions for both the N and N_F phases. This prediction could then be used to verify the phase of the LC in the cell. [5]

Using the CRC, N and N_F can be identified by observing the arising disclinations. For N, the polarity of the rubbing does not affect the LC as the phase is non-polar. Thus, the smallest possible twist of $\hat{\mathbf{n}}$ between the two surfaces will always be less than 90°, and a disclination will appear across the whole cell from left to right where the handedness of the twist changes. However, for N_F the polarity of the BCs will affect the LC at both surfaces, and for certain parts of the cell the smallest possible

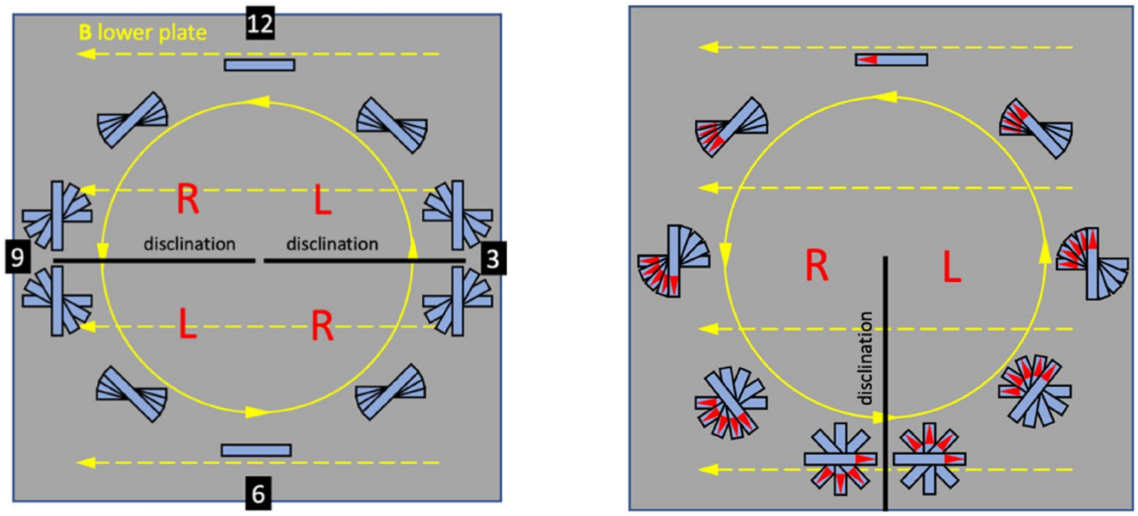

(a) N **(b)** N_F

Figure 2.8: Schematic illustrations of the cells used by Rudquist. The lower plates have a linear polar boundary condition (dashed lines), and the top plates have a circular polar boundary condition (solid lines). Further shown is the structure assumed by a N and N_F LC respectively, represented by the blue rods. The non-polar N phase twists between 0° and 90° in different parts of the cell to satisfy the BCs, while the twist required by the polar N_F phase varies between 0° and 180°. Images borrowed from Per Rudquist [5], used under Creative Commons (`http://creativecommons.org/licenses/by/4.0/`).

twist that satisfies the BCs will be up to 180° where the mutual rubbing directions are anti-parallel. This will result in one single disclination running from the middle of the cell and downwards. The configurations for both the N and N_F phases are seen in Figure 2.8. [5]

3
Methods

3.1 Cell fabrication

Cells were made from pairs of square glass substrate plates with 7.5 cm sides, which were each split into 5×5 cells. The plates had one side treated with Indium Tin Oxide (ITO), which was the one used for the inside of the cell. The ITO layer makes it possible to apply electrical fields to the cells, which is not done within this project but may be of interest in future research. The process of preparing the substrates, applying BCs and assembling the cells is described below.

3.1.1 Preparations

All plates that were to be used in the project were cleaned using part of the process Standard Clean 1 (SC1). In this process, one part H_2O_2 with 25% concentration, one part NH_4^+ with 30% concentration and five parts DI water was mixed in an ultrasonic bath and heated to 70°C. The substrates were then placed in the bath for ten minutes, and subsequently rinsed using a Quick Dump Rinse (QDR). This process was repeated four times, and the substrates were rotated in their holder between each repetition in order to clean each side equally. After four repetitions, the substrates were dried in a centrifuge and finally placed in an oven at 100°C for at least one hour.

After cleaning, some of the substrates were spin coated with the polyimide (PI) PI2610, as done by Rudquist [5]. One part PI with 10% concentration was mixed with 19 parts DMSO to achieve a final concentration of 0.5%. The mixture was stirred for three hours. A few drops of the mixture were then dropped onto each of the substrates, which were subsequently spun at 5000 rpm for 30 s using a spinner. The substrates were then soft baked at a hot plate at 100°C for 60 s, and then transferred to an oven where they were hard baked at 300°C for about three hours.

3.1.2 Boundary Conditions

Boundary conditions were applied to each substrate, using different methods. The ones which were spin coated with PI were rubbed, linearly or circularly, and the non-coated were treated with oblique evaporation of SiO_2.

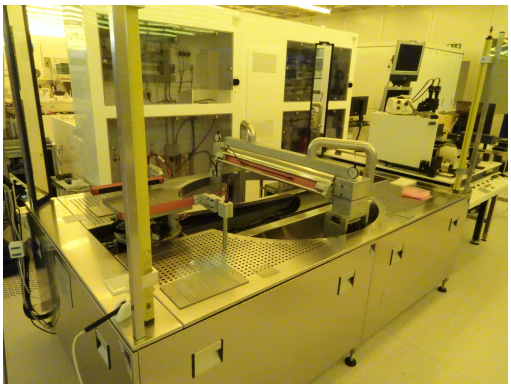

(a) Linear

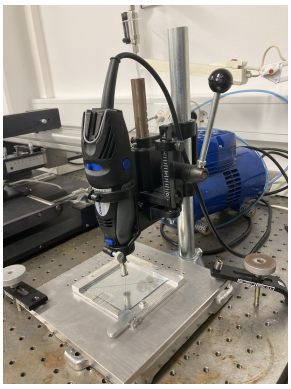

(b) Circular

Figure 3.1: The two setups used for linear and circular rubbing respectively.

3.1.2.1 Linear and Circular Rubbing

Linear rubbing was done using an LC Tec Automation buffing machine. In this process, the substrates were rubbed with a spinning cylinder covered in velvet, which creates a polar BC with a small pretilt. The effect of these BCs on RM734 was already well known, and thus these plates could be used to construct reference cells.

Circular rubbing was done using a drill mounted on a stand. A piece of velvet was taped onto the tip of the drill, which was used to brush the substrates. The substrates were placed on a holder that could be moved between 25 different positions in order to get one brush center in each cell. The setups used for both linear and polar rubbing are shown in Figure 3.1.

3.1.2.2 Oblique Evaporation

Oblique evaporation of SiO_2 was performed using an evaporator named AVAC HVC600, which can be seen in Figure 3.2. Inside the evaporator, a substrate was mounted and tilted to achieve the desired evaporation angle. The pressure inside the evaporation chamber was then pumped down to approximately $2.7 \cdot 10^{-6}$ mbar and SiO_2 was subsequently evaporated. The evaporated particles piled onto the substrate, covering it with a 200 Å layer at a rate of approximately 1 Å/s. The heating of the SiO_2 source was done using an electron beam, and the distance between the source and the substrate was approximately 40 cm.

Due to the size of the substrates being near the same order of magnitude as the distance between the source and the substrate inside the evaporator, the evaporation angle would vary a few degrees across the substrate. Because of this, the use of cells near the edges of each plate was avoided for sensitive experiments.

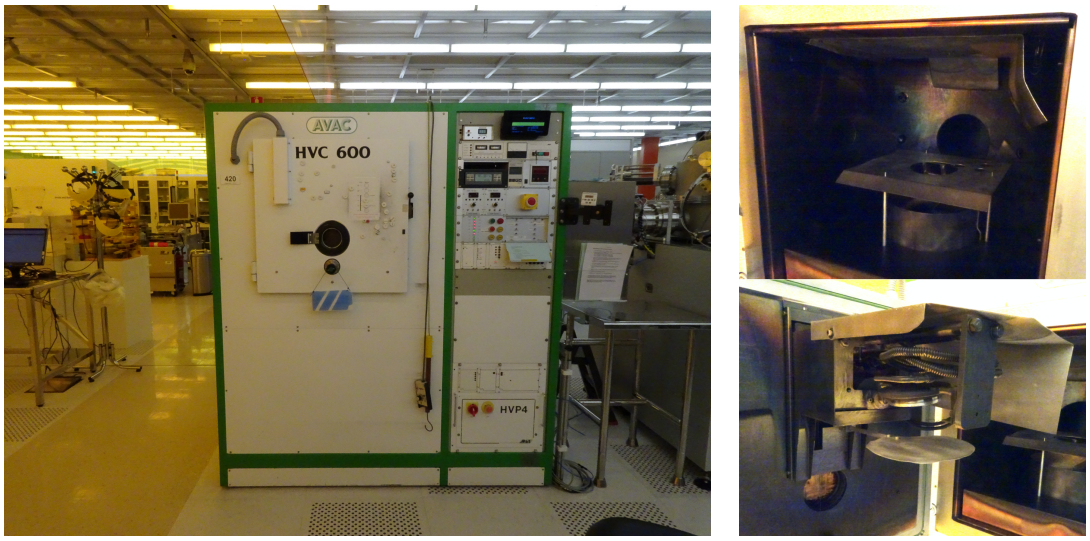

(a) Outside **(b)** Inside

Figure 3.2: The outside and inside of the AVAC evaporator. The substrate can be mounted upside down on a holder on the inside of the door, and the source is placed in the bottom of the chamber.

3.1.3 Assembly

After applying BCs, the substrates were assembled in pairs. Norland Adhesive 68 glue was mixed with 4 µm spacers to keep the distance between the plates constant. The glue was then dispensed in the pattern seen in Figure 3.3 on one of each pair of plates using a glue dispenser. For each pair, the plate chosen to dispense the glue on was the one considered easiest to replace in case the dispenser did not work properly.

After dispensing the glue, an aligner and assembler from Ciposa was used to align and assemble the plates. The glue was then fixated using UV light for about 4 s. Subsequently, the cells were vacuum packed in a plastic bag, and further fixated using UV light for ten minutes.

Once the glue was fixed, each pair of plates were cut into 1.25 cm wide and 1.25 cm long cells. This was done by using a diamond cutter to mark the lines along which the cells should be cut, and then carefully cracking the glass.

3.1.3.1 Different Types of Cells

The different cells which can be constructed using the methods described above can be seen in Figure 3.4.

The standard demo cells, where both plates were linearly rubbed, were made with the rubbing both parallel, anti-parallel and at a 90° angle. The double evaporated cells (DEC) were made in two sets with the evaporation direction parallel and anti-parallel respectively. Both sets had the evaporation angle $\alpha = 30°$.

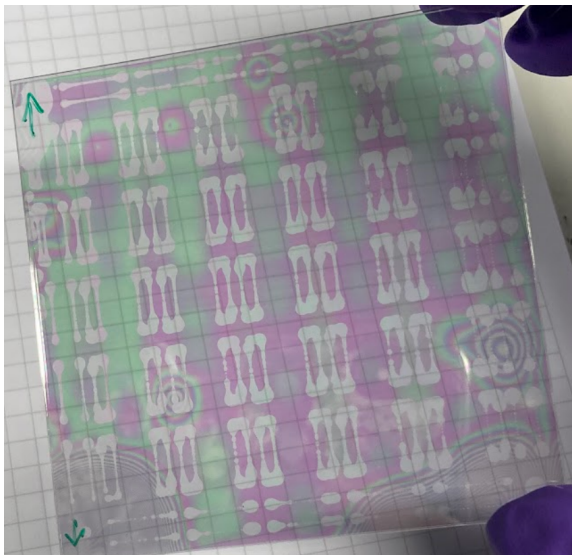

Figure 3.3: Two glass plates glued together to make a set of 5×5 cells. The pattern made by the glue dispenser is clearly visible.

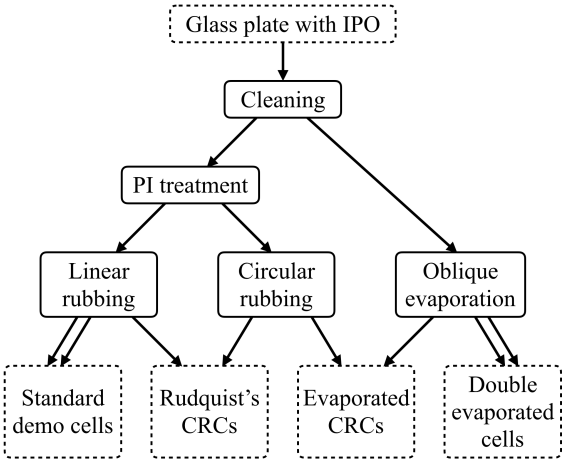

Figure 3.4: Flowchart showing the procedure to produce different types of cells. All types of cells shown in the flowchart were used in this project, with the main focus on ECRCs.

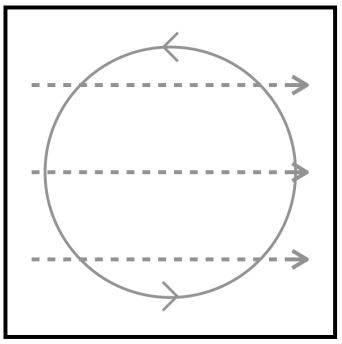

Figure 3.5: Schematic illustration of the ECRC. The solid line show the circular rubbing direction on the bottom plate, and the dashed lines show the evaporation direction on the top plate. Note that the evaporation direction is not generally equivalent to the alignment of $\hat{\mathbf{n}}$ at the surface.

The most notable type of cell used in this project is the evaporated CRCs (ECRC), which is shown in Figure 3.5. As seen in the flowchart in Figure 3.4, they consist of one circularly rubbed PI-coated plate and one treated with oblique evaporation of SiO_2. The ECRCs were made in three sets, with $\alpha = 30°$, $\alpha = 45°$ and $\alpha = 80°$. The evaporation angles were chosen based on the alignment of E7 described by Jägemalm [6], such that the boundary conditions would be expected to be polar in some cells and non-polar in others.

3.2 Studying the Cells

Each cell was filled with LC, one at a time. This was done by placing the cell on a hot stage with a temperature corresponding to the LC being in the isotropic phase. For RM734 the temperature was 190°C, and for E7 it was 60°C. A drop of LC was then placed on the side of the cell and injected via capillary force. The hot stage, with the cell still inside, was then placed under a microscope for studying. The hot stage had a small hole in the bottom and lid, allowing for studying using POM while keeping the sample heated. Due to strong memory effects in the LC, which is shown in further detail in chapter 4, the LC was not allowed to crystallize or enter the N_F phase between filling and studying.

The temperature of each sample was decreased and continuously controlled using the hot stage, and the appearance of the samples were studied. Both the sample and the polarizers in the microscope were rotated in order to determine the alignment of $\hat{\mathbf{n}}$ in different domains. Details and results from these observations are described in chapter 4.

4
Results and Discussion

The results of this thesis can be split into two main parts; Alignment in ECRCs, and alignment in DEC. These are both described in this chapter. Before these are presented, some demonstration cells are presented, which were used as references to recognize the different phases of RM734.

4.1 Demonstration Cells

In order to learn how to recognize the N and N_F phases, ordinary linearly rubbed cells were used. Three different types were used, where the rubbing directions on the two opposite sides were parallel, normal or anti-parallel to each other.

In the cell with parallel rubbing, there was no notable difference between the N and N_F phases, as seen in Figure 4.1. When the rubbing was parallel to one of the polarizers, both phases resulted in black images, as expected based on the theory described in Section 2.3.1. When rotated 45° from the dark state, the cells appeared smooth and uniform in colour. The colour varied gradually with the temperature of the sample, due to its effect on the birefringence of the sample. The colour also changed notably at the phase transition between N and N_F. This indicates that the birefringence changes at the transition. Apart from this, no clear difference was observed between the two phases.

The cell where the surfaces had been rubbed in directions normal to each other gave results similar to the previous type, as both phases behaved similar to each other. The results can be seen in Figure 4.2. As described in Section 2.3.1, the cell let through approximately white light when placed between crossed polarizers so that the rubbing directions were parallel to the polarizers. When the cell was rotated 45° from the white state, some colour was seen. Just as for the previous type of cell, the colour depended on the birefringence, and changed with both temperature and phase.

The cell with anti-parallel rubbing were the only ones appearing drastically different in the two phases, as seen in Figure 4.3. The N phase in this cell appeared identical to the cell with parallel rubbing, which was expected due to the phase being non-polar. In the N_F phase, however, two domains appeard, divided by a zigzag-shaped border. The domains had the same colour between crossed polarizers, but changed to different colours when one polarizer was rotated. If the polarizer was

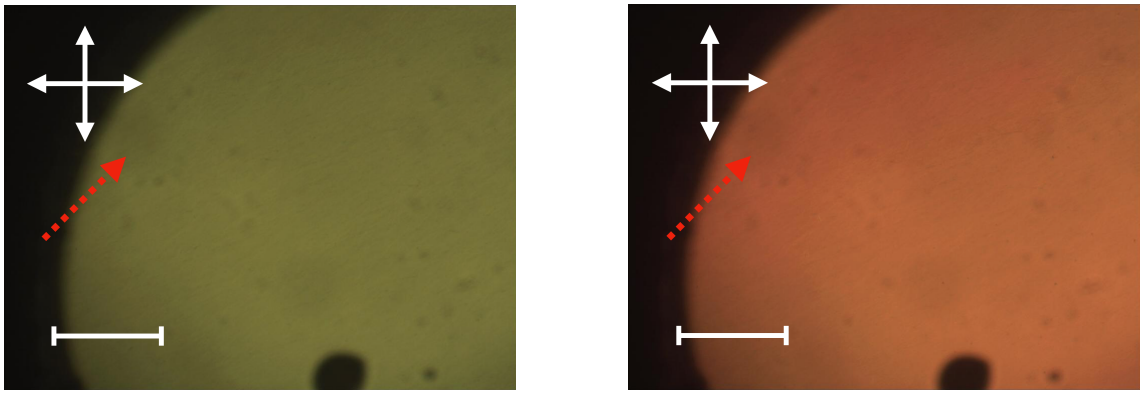

(a) N **(b)** N_F

Figure 4.1: RM734 in the N and N_F phases in a cell where both surfaces have been rubbed in the same direction. Apart from a change in colour, there is no notable difference between the two cases. The white arrows show the polarizers and the red dashed arrows show the rubbing direction. The scalebar in the lower left corner is 0.5 mm.

instead rotated in the opposite direction, the two domains would switch colours. The behavior indicates twist domains with opposite handedness. This is expected, since the N_F phase is polar and a 180° twist would be necessary to satisfy the BCs.

4.2 ϕ in ECRCs

The alignment of an LC on an evaporated surface was studied in terms of the angle ϕ, which is described in Sections 2.2.2 and 2.4.2. This was done in detail in the N phase for both E7 and RM734, and partially in the N_F phase for RM734. The main part of the project focused on the alignment in ECRCs, and the results are presented below for the three cases.

4.2.1 E7

The value of ϕ for E7 at different temperatures and different α has previously been studied by Pontus Jägemalm [6]. Since this project uses CRCs rather than two evaporated plates put together, it was of interest to determine wether or not this changed the behavior of ϕ compared to Jägemalm's results.

Cells with one circularly rubbed substrate and one obliquely evaporated substrate were put together and filled with E7. At $\alpha = 30°$ and $\alpha = 45°$, the angle $\phi_\alpha = 0°$ turned out to be constant at all temperatures below the transition temperature from isotropic to N, with some fluctuation but no clear temperature dependence.

For $\alpha = 80°$, a temperature dependence could be seen. At temperatures just below the transition temperature from isotropic to N $\phi_{80°}$ was 90°. However, with

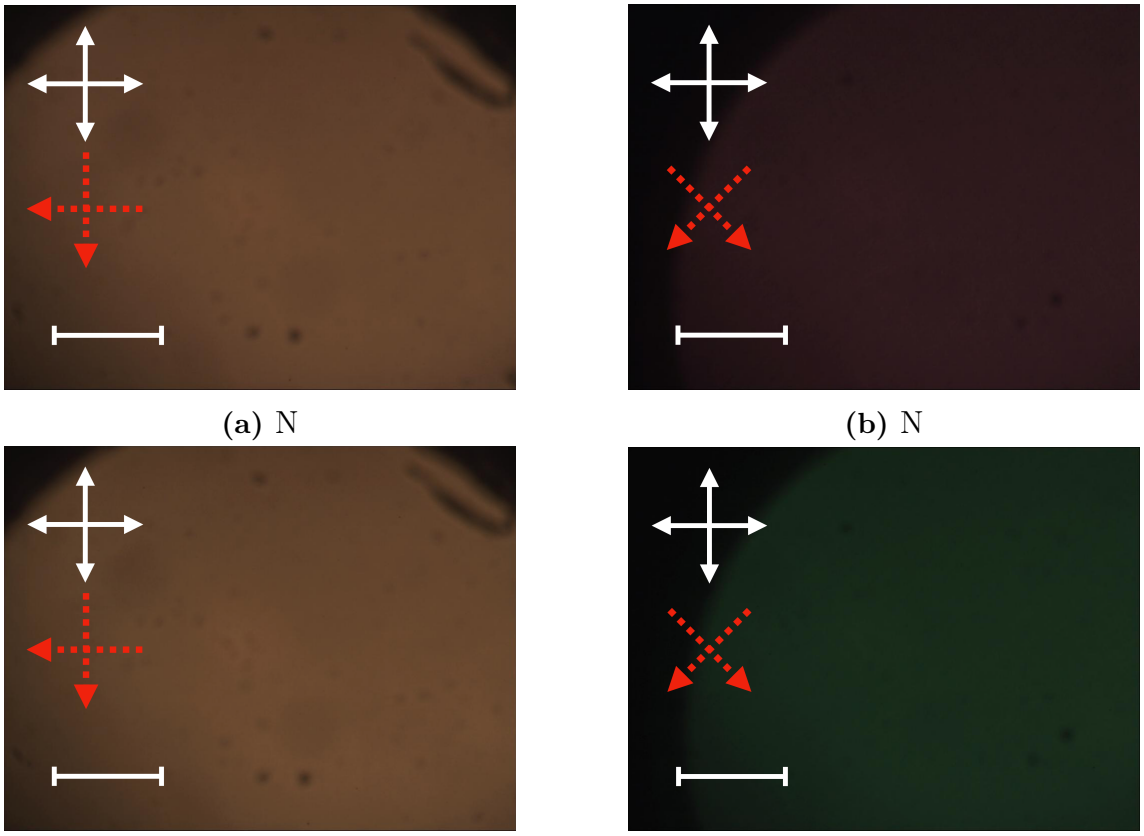

(a) N **(b)** N

(c) N_F **(d)** N_F

Figure 4.2: RM734 in the N and N_F phases in a cell where the two surfaces have been rubbed in directions normal to each other. Apart from a change in colour in the images where the rubbing directions are not parallel to the polarizers, there is no notable difference between the two cases. The white arrows show the polarizers and the red dashed arrows show the rubbing directions. The scalebar in the lower left corner is 0.5 mm.

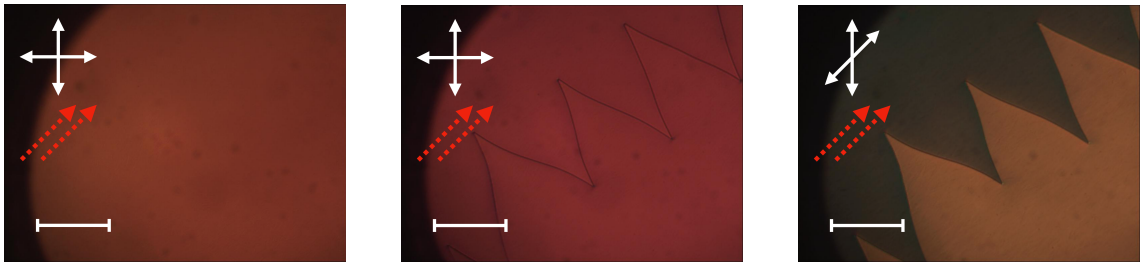

(a) N **(b)** N_F **(c)** N_F

Figure 4.3: RM734 in the N and N_F phases in a cell where both surfaces have been rubbed in opposite directions. In the N_F phase, two domains appear with opposide handedness, leading to them having different colours when the polarizers are not normal to each other. The shape of the border between the two domains has a shape which is characteristic for 180° twists in the N_F phase. The white arrows show the polarizers and the red dashed arrows show the rubbing direction. The scalebar in the lower left corner is 0.5 mm.

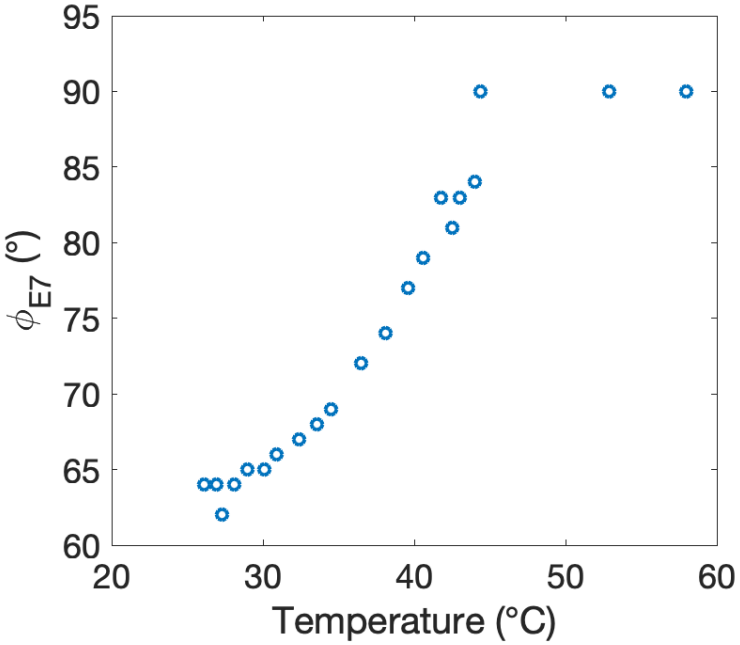

Figure 4.4: Relation between temperature and ϕ for E7 in an ECRC with $\alpha = 80°$.

decreasing temperature it fell, before stabilizing at around $\phi_{80°} = 64°$, as seen in Figure 4.4. Based on Jägemalm's study, it would be expected to decrease even further, reaching $\phi_{80°} = 0°$ at room temperature. A possible explanation to why it does not is that a balance is reached where a further decrease of $\phi_{80°}$ would cause a twist which would in turn result in an increase of elastic energy, as explained in Section 2.1.2. There may also be some differences between the evaporation methods used. The thickness of the evaporated layer is similar to that of Jägemalm's study, but may vary due to differences in calibration. The structure of the layers may also vary, partially since Jägemalm uses SiO_x instead of SiO_2, and partially due to differences between different evaporation tools. However, the most likely is that there is a production error that originates the evaporation stage, where the evaporation angle α produced by AVAC is actually $5 - 10°$ smaller than intended. This would make the results from the experiments agree with Jägemalm, and the evaporator used to make the cell has a known such uncertainty. Some hysteresis was also found in the temperature dependence of $\phi_{80°}$, which is in agreement with Jägemalm.

To minimize the twist of $\hat{\mathbf{n}}$ in each part of the cell, which would be energetically favourable due to the elasticity of the LC, two new disclinations would be expected to appear in addition to the original two once $\phi_{80°}$ starts decreasing, as illustrated in Figure 4.5. However, in the experiments only two disclinations were visible regardless of $\phi_{80°}$, as seen in Figure 4.6. This implies that $\hat{\mathbf{n}}$ rotates one way across each half plane of the cell. This can be confirmed by rotating the cell, since a non-twisted $\hat{\mathbf{n}}$ will lead to light extinction when parallel to one of the polarizers.

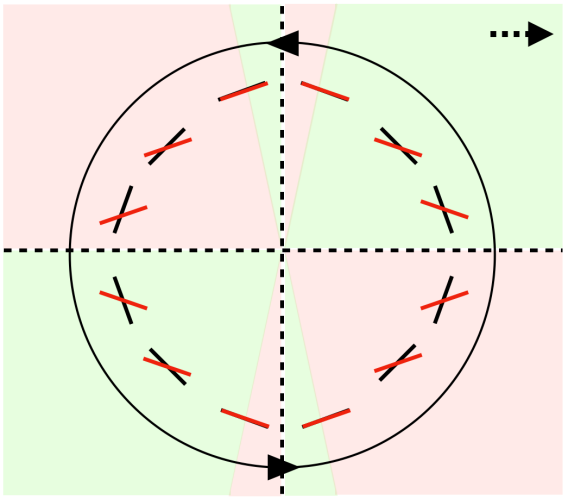

Figure 4.5: Prediction of $\hat{\mathbf{n}}$ for N in an ECRC when $\phi = 19°$. The dashed lines represent disclinations, and the dashed arrow represents the evaporation angle. The circle shows the circular rubbing. Short black and red lines show $\hat{\mathbf{n}}$ at different circle sectors near the rubbed and evaporated surfaces respectively, and the red and green fields represent the handedness of the minimum twist between them, where greein is right handed and red is left handed. The energy required to form disclinations and any effect arising from pretilt at the surfaces are not taken into account in this model. More similar predictions for different values of ϕ can be found in Appendix A.

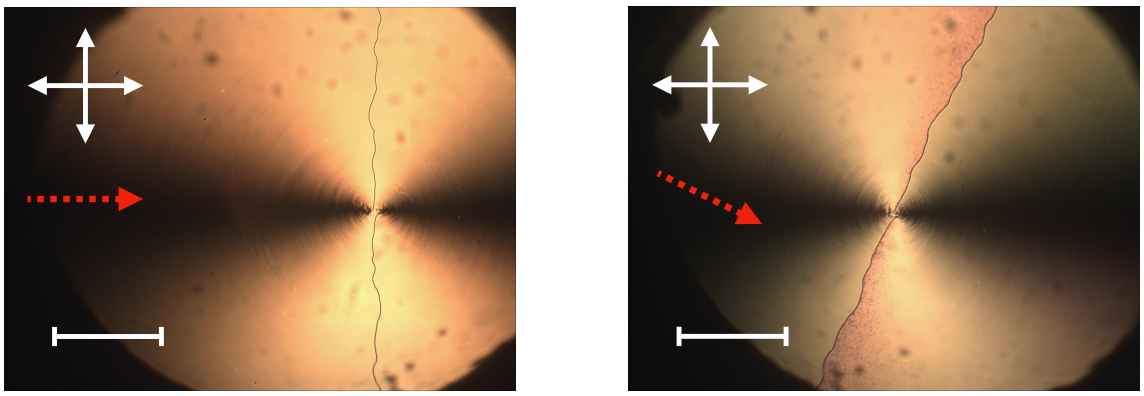

(a) 58.0°C **(b)** 26.1°C

Figure 4.6: E7 in an ECRC with $\alpha = 80°$ viewed between crossed polarizers at different temperatures. The disclinations have not moved between the two images, but the sample has been rotated in order to achieve light extinction and thus determine $\phi_{80°}$. The white arrows show the polarizers and the red dashed arrows show the evaporation direction. The scalebar in the lower left corner is 0.5 mm.

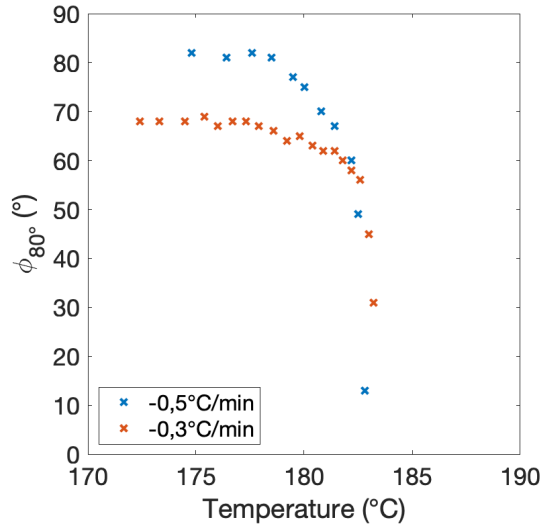

Figure 4.7: Relation between temperature and ϕ at different cooling rates and $\alpha = 80°$. Once a final value of ϕ had been reached in each cell it would stay constant regardless of any temperature changes.

4.2.2 RM734 in N

Cells with the same BCs as above were filled with RM734 in order to compare ϕ for the different LCs. For RM734, some memory effects appeared to affect the results, as the experiment could not be repeated with the same results without filling a new cell.

Two cells with $\alpha = 80°$ were filled at 190°C and then cooled down at different rates. Both quickly converged at high ϕ, but the one cooling down at a higher rate converged at a slightly lower value than the other, as seen in Figure 4.7. When temperature was then increased, ϕ stayed constant, indicating a memory effect which was not present in the case of E7.

More cells were filled at 190°C, and the temperature was then decreased as fast as the hot stage allowed to different temperatures for each cell. The cells were then left at that temperature for some time, and ϕ was measured. The results from these measurements, which can be seen in Figure 4.8, were much closer to the expected ones. Just like in the case with E7, lower temperatures generally meant smaller ϕ. After about 10 minutes the temperature was changed, but ϕ remained constant for each cell.

In contrast to the case with E7, RM734 in ECRCs and in the N phase resulted in four different fields with alternating directions of $\hat{\mathbf{n}}$ and disclinations between them, as seen in Figure 4.9. The configuration was similar to the one predicted in Figure 4.5, which was confirmed by rotating the sample between crossed polarizers. The left and right disclinations did not generally point horizontally, but rather a bit towards one of the vertical disclinations. These domains are described in further detail in Section 4.2.4.

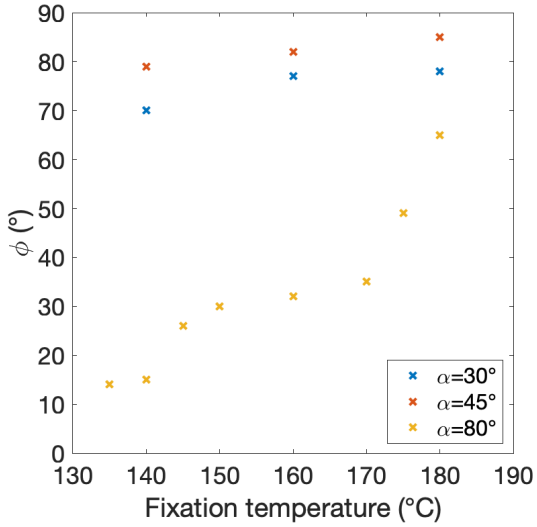

Figure 4.8: Relation between fixation temperature and the values of ϕ for different α. Cells were filled at 190°C, and cooled down to the fixation temperature before measuring ϕ. Near the phase transition temperatures $\hat{\mathbf{n}}$ stops being affected by the evaporated BCs, leading to ϕ being undefined.

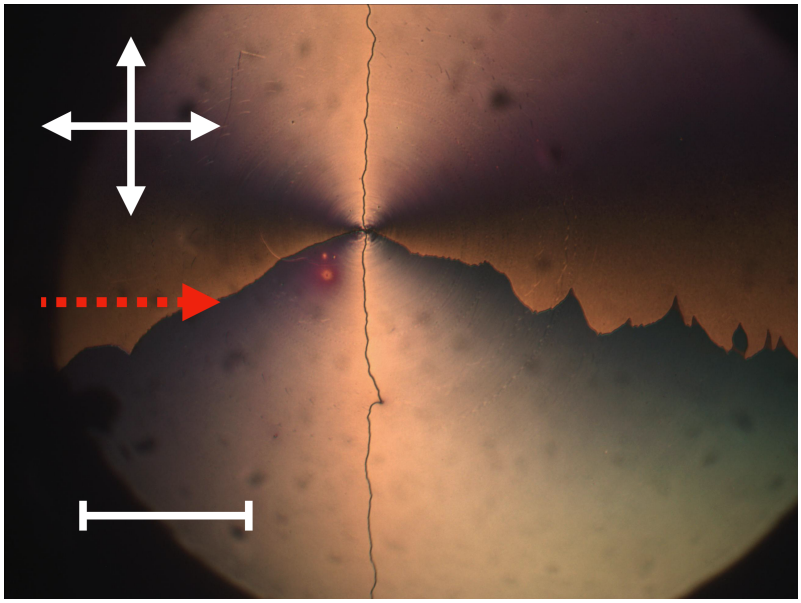

Figure 4.9: RM734 in an ECRC with $\alpha = 30°$ viewed between crossed polarizers at 150°C. The white arrows show the polarizers and the red dashed arrows show the evaporation direction. The scalebar in the lower left corner is 0.5 mm. The cell is divided into four domains, where the domain borders are created by kinks in the alignment of $\hat{\mathbf{n}}$ at the obliquely evaporated surface.

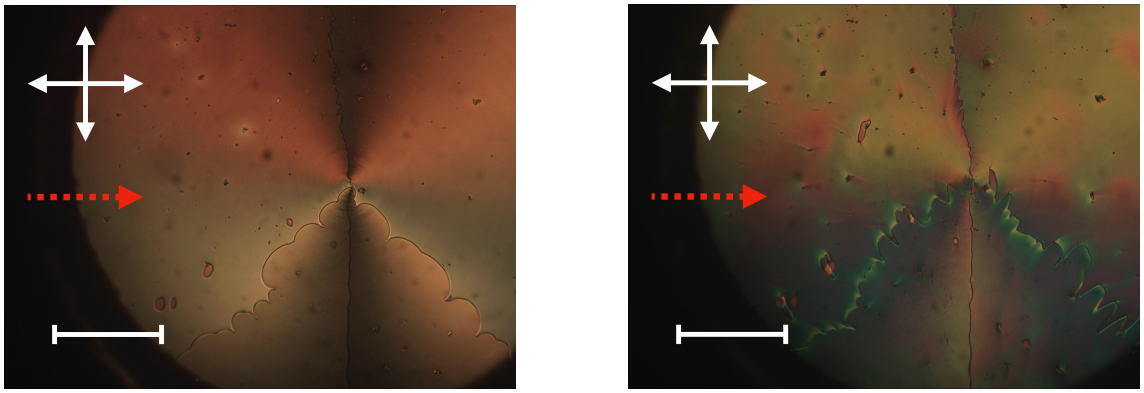

(a) 160°C, N **(b)** 125°C, N_F

Figure 4.10: RM734 in an ECRC with $\alpha = 80°$ viewed between crossed polarizers at two different temperatures. The white arrows show the polarizers and the red dashed arrows show the evaporation direction. The scalebar in the lower left corner is 0.5 mm. The cell is split into four domains. The domain borders running from the middle to the top and bottom are identical in both images. The sideways borders are more uneven in the N_F phase than in the N phase.

4.2.3 RM734 in N_F

After the transition from the N to the N_F phase, it becomes much more difficult to determine the value of ϕ. This is due to a number of reasons. The main reason is because there is not always a part of an ECRC where $\hat{\mathbf{n}}$ is parallel on both surfaces of the cell. The polarity of the BCs and the phase leads to part of the cell needing a 180° twist in $\hat{\mathbf{n}}$ to conform to the BCs. These domains with large twist are generally the larger part of the cell, and the domains with smaller twists are not guaranteed to be large enough to cover the part where it would be possible to achieve no twist. It is also common that it is located near the border, making it difficult to determine the angle properly.

Another factor that makes it difficult to measure ϕ in the N_F phase is that the twist in the cells seems to fluctuate across the surface in a way that it does not in the N phase. This can be seen in Figure 4.10b, where the colour varies between red and green across each domain in seemingly random patterns. This may stem from a tendency to twist due to electrostatic effects in N_F as predicted by Kachaturyan in 1975 [18]. This may cause $\hat{\mathbf{n}}$ to wobble in the bulk to achieve its preferred pitch with altering handedness. However, this explanation is only a hypothesis and has not been shown within this thesis.

In each domain in the cell ϕ appears to keep the same sign as in the N phase, due to the fixation that happens in the N phase. There is only one line across the cell where $\hat{\mathbf{n}}$ changes substantially, which is described further in Section 4.2.4. This is along one line where change is necessary when transitioning from a non-polar phase into a polar phase to conform to the polarity of the BCs.

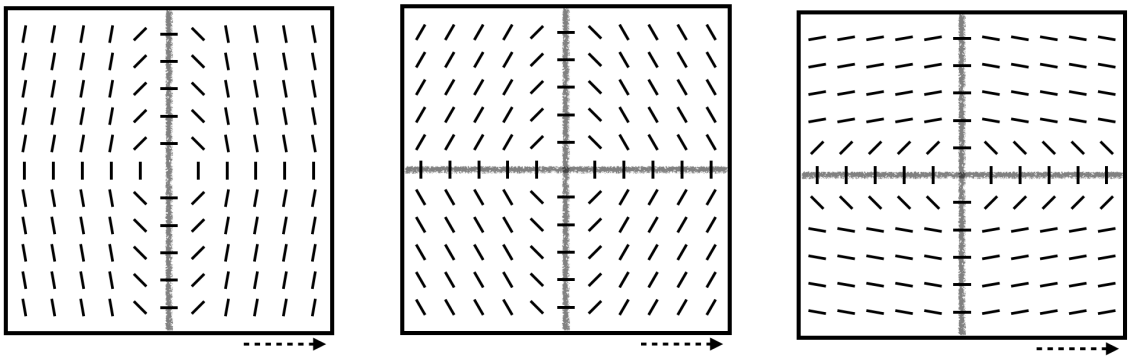

(a) $\phi \approx 0°$ **(b)** $\phi \approx 45°$ **(c)** $\phi \approx 90°$

Figure 4.11: Orientations of $\hat{\mathbf{n}}$ on the evaporated surface of the ECRC at different values of ϕ in the N phase, when ϕ starts at 90° and decreases gradually. The gray lines represent kinks in $\hat{\mathbf{n}}$ on the surface, and may coincide with twist disclinations. The horisontal lines are drawn the way they would appear in an optimal cell with no pretilt or defects, but will in reality point slightly downwards. The dashed arrows represent the evaporation direction.

Based on the few cases where it has been possible to measure ϕ, it seems likely that its value stays approximately the same in the N_F phase as in the N phase, making it possible to control the N_F phase by letting it fixate at a chosen temperature in N. However, the difficulty in measuring ϕ in the N_F phase makes it impossible to be sure based only on the results from this project. The possibility that the fixation disappears or that ϕ may even change discontinuously at the transition can not be ruled out. Measurements of how ϕ in the N_F phase depends on temperature were not made, since including factors such as time and temperature in the experiments would increase the complexity of the problem even further.

4.2.4 Domains and Memory Effects

A notable result that makes the results distinctly different from Rudquist's CRCs, which are described in Section 2.4.3, is the division of the evaporated surface in four domains. In Rudquist's study, $\hat{\mathbf{n}}$ was aligned the same across the whole linearly rubbed surface, since $\phi = 0$ for rubbed surfaces. Thus, the only lines visible in the results were twist disclinations in the bulk of the LC. Since this is not true for an evaporated surface, the cell will be divided into domains where $\hat{\mathbf{n}}$ has different surface alignments. These domains are shown in Figure 4.11. The orientation of the director at the domain boundaries was confirmed using a compensator.

When a cell is near the transition temperature from isotropic to N, and has not been cooled down before, the value of ϕ is near 90°. This means that $\hat{\mathbf{n}}$ at the evaporated surface is oriented the same way across the whole cell. However, a twist disclination is necessary in two places to keep the alignment at both the evaporated and rubbed surface, and this happens in the two places where $\hat{\mathbf{n}}$ at the two surfaces form a right angle, splitting the cell in two halves. This disclination is typically located on the evaporated surface. Because of this, the disclination will become

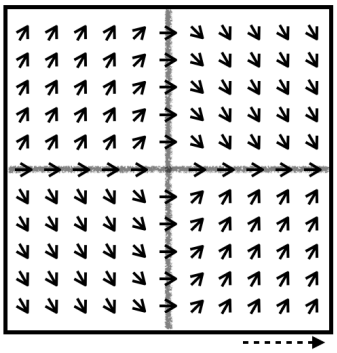

Figure 4.12: Expected orientation of $\hat{\mathbf{n}}$ at the evaporated surface of an ECRC, with $\phi \approx 45°$. Note that the orientation is the same as in N on all parts of the cell except for on the horisontal grey lines, where it has been rotated 90° in order to create a continuous transition between the upper and lower domains.

fixed and stay in the same position no matter what else happens to the cell [19]. All studied cells passed through this state since they were filled in the isotropic state.

In the cases where ϕ was allowed to grow significantly smaller than 90°, each half of the cell split into two domains, where $\hat{\mathbf{n}}$ rotated in either positive or negative direction in order to minimize the required twist energy to satisfy the BCs. In theory, these domains should be equal in size, but in practice they were not. A hypothesis is that it depends on pretilt. The pretilt should in turn depend on ϕ [7]. Between these four domains, lines form marking kinks in $\hat{\mathbf{n}}$ on the evaporated surface. Whether or not each line is also a twist disclination or only a kink in $\hat{\mathbf{n}}$ depends on ϕ. Larger values of ϕ give a twist disclination at the two old lines, and only a kink at the new lines, while smaller values of ϕ do the opposite. Mid-range values of ϕ do not necessarily have to give twist disclinations anywhere, as the director is approximately a circle on both surfaces.

In the cases where ϕ continues to decrease to values near 0°, $\hat{\mathbf{n}}$ is once again oriented the same way across the whole evaporated surface. However, since the lines described above are all fixed, the four domains still remain. In this case, the lines towards the sides will be twist disclinations, and the vertical ones which appeared first will only be small kinks in $\hat{\mathbf{n}}$ on the surface.

If the temperature is increased after any of these disclinations have formed, the formation of the lines described above will not be reversed, since they are located on the surface of the cell rather than in the bulk of the LC. The vertical lines stay identical, and within the N phase the sideways lines will do the same. However, at the transition to N_F, the new phase will make the sideways lines change slightly, as seen in Figure 4.10. This is likely due to the polarity of the new phase, which makes the previous configuration insufficient to satisfy the polar BCs, as seen in Figure 4.12.

After the transition from N to N_F two additional lines may appear, dividing each

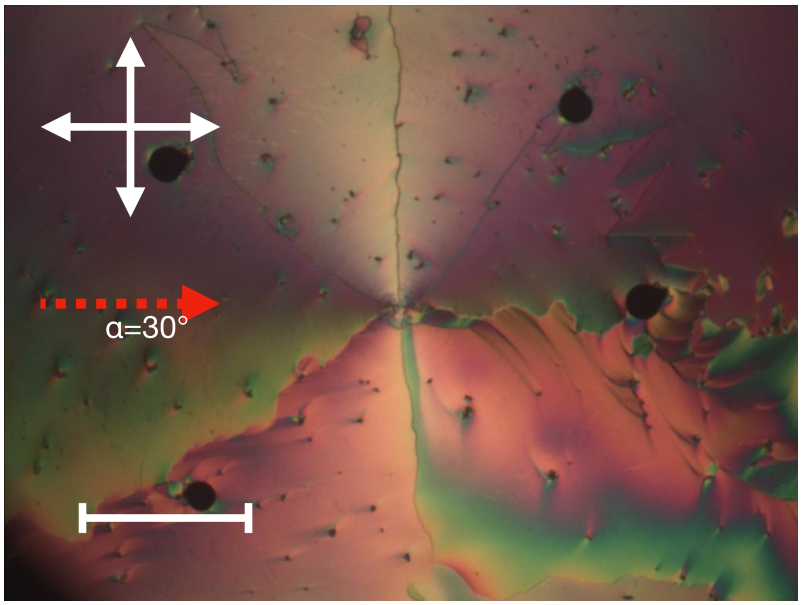

Figure 4.13: RM734 in an ECRC with $\alpha = 30°$ viewed between crossed polarizers at 125°C. The white arrows show the polarizers and the red dashed arrows show the evaporation direction. The scalebar in the lower left corner is 0.5 mm. In addition to the four domain borders seen in previous photos, two twist disclinations have appeard pointing upwards to the sides.

of the two larger domains into two domains, as seen in Figure 4.13. No detailed research has been made regarding when this happens or not, but it appears to be more likely to happen for smaller values of α. These lines are twist disclinations between domains with right handed and left handed 180° twists, and have a zigzag shape similar to what was seen in the anti-parallel demonstration cell in Figure 4.3. The disclinations are typically located in the bulk of the cell rather than on a surface, which can be known since it disappears at the transition back to N without leaving traces [19]. This is expected, since ϕ does not switch sign at this disclination, and in that case locally diverging from the BC would increase the energy of the system more than necessary.

4.3 Double Evaporated Cells

In order to compare the results from the ECRCs with a simpler geometry, two sets of cells with obliquely evaporated SiO_2 on both surfaces were made. Both sets used $\alpha = 30°$. One set had parallel evaporation directions, and the other anti-parallel. The cells were mainly used to study the behavior of RM734 during the transitions between the N and N_F phases. Since the BCs on the surfaces were constant across each cell, the alignments were the same across each surface and no domain borders appeared.

From the ECRC experiments we know that $\alpha = 30°$ gives $\phi > 70°$, as seen in Figure 4.8, which in turn leads to the BCs being almost non-polar. Because of

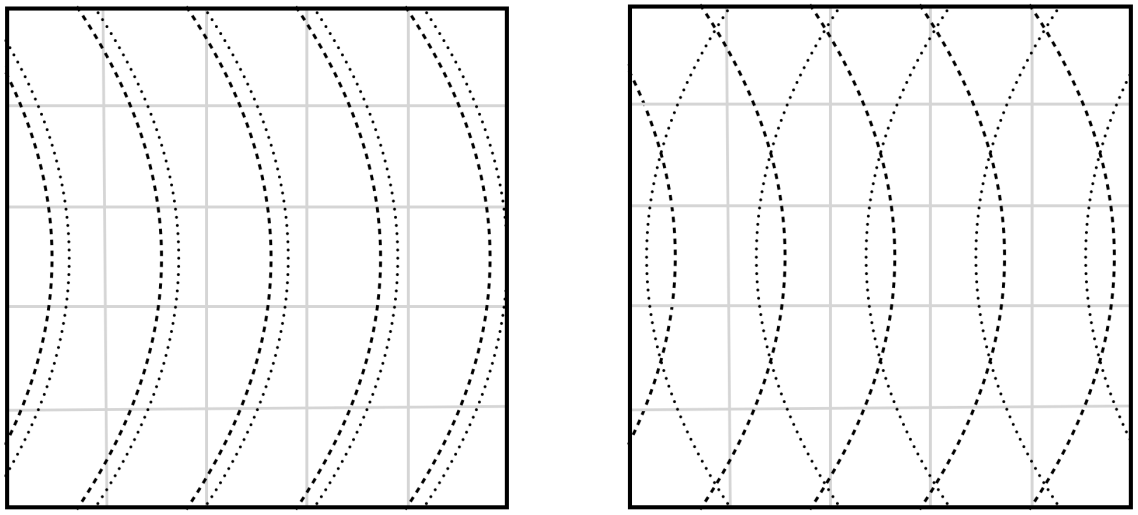

(a) Parallel **(b)** Anti-parallel

Figure 4.14: Schematic illustrations of the boundary conditions in the two sets of DEC. The gray lines show the divisions of each pair of plates into 25 cells. The dashed and dotted lines are normal to the evaporation direction on the top and bottom plates respectively, showing how $\hat{\mathbf{n}}$ will align in the case where $\phi \approx 90°$. In the case with parallel evaporation directions, the alignment is parallel in all cells. In the anti-parallel case, only the middle row has parallel alignment while the other rows have an angle between the top and bottom BCs.

this, both sets of cells showed the same behavior. One exception to this was for cells far from the middle of the 5×5 sets of cells. This was caused by the large variation in evaporation direction across the substrate plates in the evaporator, which made edge cells have different angles between the BCs, as shown in Figure 4.14. However, cells taken from the middle row of the sets had almost perfectly anti-parallel BCs, and behaved the same as those from the parallel sets.

The transition cycle between the N and N_F phases is shown in Figure 4.15. At the top and bottom of the figure, the stable configurations of $\hat{\mathbf{n}}$ in the two phases are shown, and on the sides are the different states that the cell goes through throughout the phase transitions.

A cell in the N phase has a homogeneous non-twisted $\hat{\mathbf{n}}$ throughout the whole cell. At the transition to the N_F phase, the LC initially assumes a polar non-twisted homogeneous state, with some coloured zones near air bubbles due to a small twist being introduced at the bubble edges. However, electrostatic effects in the polar phase cause the LC to begin a spontaneous 180° twist to decrease the energy of the system. The twist seems to have no clear preferred handedness since the medium is achiral, and begins to spread with different handedness from edges and defects, thus forming red and orange regions when viewed between crossed polarizers. This is all in agreement with the theoretical results from Kachaturyan [18], where the N_F phase is predicted to twist spontaneously dispite not being chiral. It also appears similar

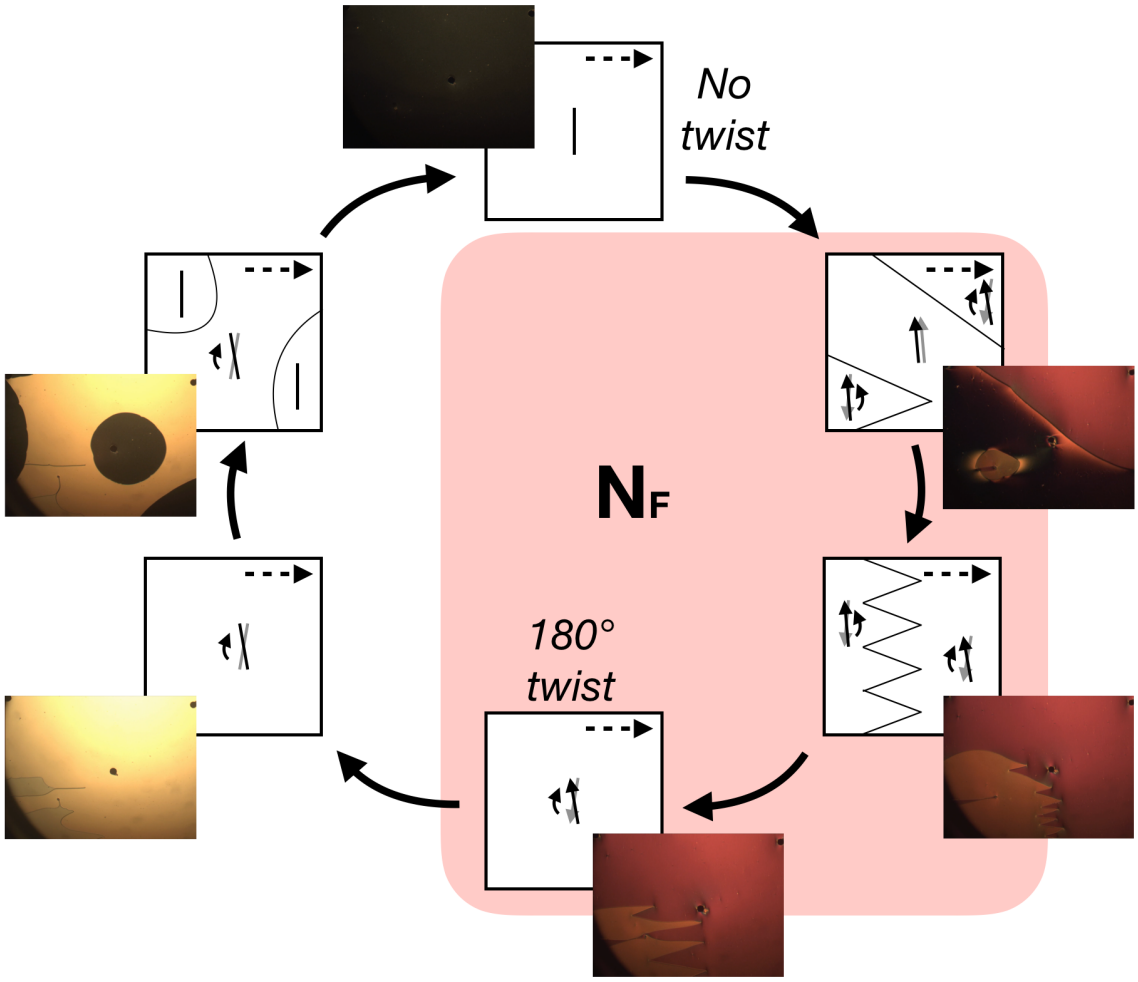

Figure 4.15: A map showing the states RM734 passes through during the phase transitions between N and N_F in a cell with parallel non-polar linear BCs. The states within the pink are in the N_F phase, and the rest are in the N phase. The evaporation direction is towards the right in all cases. Each state is also photographed between crossed polarizers.

to recent experimental results by Yu et al regarding the alignment of the N_F phase on rubbed surfaces [3]. However, twisted LCs are very sensitive to different angles between BCs, and since the BCs are never perfectly aligned, one twist generally has lower energy than the other. It is also likely that there is a difference in energy near the surfaces depending on whether $\hat{\mathbf{n}}$ twists towards or away from the evaporation direction. Thus, one twisted domain will have lower energy than the other, and once they meet the one with lower energy will push the other back, eventually taking over the entire cell. This will lead to the stable twisted state of the N_F phase.

At the transition from N_F to N, a similar process takes place. Initially, the twist created in N_F does not disappear. Instead, the LC assumes an unusual case of N with an approximately 180° twist, which may be divided into domains with opposite handedness if the transition takes place before the lowest energy N_F state has completely taken over the cell. Eventually, domains without twist will start to spread from the edges and defects in the cell, returning the cell to its original stable non-twisted N state. This relaxation process appears to be connected to temperature, and can be slowed down substantially by interrupting the heating process right after the phase transition.

5
Conclusion

This thesis presents a qualitative description of how RM734 in the N and N_F phases aligns on a surface treated with oblique evaporation of SiO_2. The results indicate that $\hat{\mathbf{n}}$ will not generally align in parallel with or normal to the evaporation plane, but instead take a position in between these two cases. The angle ϕ between $\hat{\mathbf{n}}$ and the evaporation direction is shown to have a temperature dependence similar to that of the material E7. However, ϕ is also shown to have a time dependence, where it will fixate at a certain value after some time in the N phase.

The characteristic domains in an ECRC filled with RM734 are described for the first time. The appearance of these cells is fundamentally different from that of Rudquist's CRCs, and the difference mainly arises from the fact that $\hat{\mathbf{n}}$ changes direction in different domains. This results in kinks in $\hat{\mathbf{n}}$ on the evaporated surface, which do not move or disappear once they are formed.

Finally, $\hat{\mathbf{n}}$ is mapped throughout the transition cycle between N and N_F. In doing this, the N_F phase is also shown to spontaneously twist due to electrostatic effects. As the medium is not chiral, the helix which is formed will not have a preferred handedness to minimize the energy in the system. Instead, the handedness is either random or determined by the surrounding BCs.

5.1 Applications

As the N_F phase is relatively new, it is still unknown what the uses for the phase will be. At this stage, researchers are mapping the properties of the phase. Future applications may appear when a different project calls for a specific property or set of properties that RM734 turns out to have. For example, this project confirms a previous hypothesis that the N_F phase has a spontaneous twist without being chiral, a property which is otherwise difficult to find in LCs.

A property that might turn out to be of interest technologically is the shown time dependance of ϕ. This thesis shows that the history of a cell affects the current state, and thus different temperature sequences could be used to manipulate otherwise identical cells to appear differently. If this effect is studied and mapped with more detail, it could potentially be used in some type of temperature controlled devices which take into account both current and past temperatures.

It appears unlikely that the N_F phase will be useful in displays in ways similar to N. This is mainly due to its tendencies to form domains with chaotic borders in geometries where the N phase would simply form one large homogeneous domain. Another reason is that the LCD market does not have much incentive to improve further, since there are already displays available with both remarkably high speed and a resolution high enough for the human eye not to notice the pixels.

5.2 Further Research

This thesis lays the groundwork for further research regarding the alignment of RM734 on SiO_2. Based on the results presented above, a number of questions arises. A few of these questions are listed below, and each one of them may in itself be a sufficient scope for a new research project.

- Make more accurate quantitative measurements of the fixation time of ϕ in N.
- Is there a temperature dependence for ϕ in N_F, similar to that seen in N?
- Does ϕ fixate in N_F even if it has not done so in N?
- Is the change in ϕ at the transition from N to N_F continuous?
- Are there conditions under which ϕ switches sign locally?
- How large is the pitch arising from the spontaneous twist in N_F?
- What factors affect whether or not the two pure twist disclinations appear in N_F in an ECRC?
- What factors affect the relative size of the four domains seen in an ECRC?
- How does the thickness of the evaporated SiO_2 layer affect the results?
- Why does RM734 in the N phase split the ECRCs into four domains, when E7 only splits it into two?
- If a material is found in the future that can transition directly from isotropic to N_F, does that alter the behaviour of ϕ?

Many of the questions can be expected to be more complex than they appear at first glance, especially since RM734 and the N_F phase are still largely unexplored. It is probably advisable to cover the first question before attempting many of the others, since an unknown fixation time can make other results difficult to interpret. At the same time, different factors may interact with each other and they are likely to all be connected.

Bibliography

[1] Richard J. Mandle, S. J. Cowling, and J. W. Goodby. "A nematic to nematic transformation exhibited by a rod-like liquid crystal". In: *Phys. Chem. Chem. Phys.* 19 (18 2017), pp. 11429–11435. DOI: 10.1039/C7CP00456G. URL: http://dx.doi.org/10.1039/C7CP00456G.

[2] Richard Mandle, Stephen Cowling, and John Goodby. "Rational Design of Rod-Like Liquid Crystals Exhibiting Two Nematic Phases". In: *Chemistry - A European Journal* 23 (Aug. 2017). DOI: 10.1002/chem.201702742.

[3] Jeong-Seon Yu et al. "Alignment properties of a ferroelectric nematic liquid crystal on the rubbed substrates". In: *Soft Matter* 19 (13 2023), pp. 2446–2453. DOI: 10.1039/D3SM00123G. URL: http://dx.doi.org/10.1039/D3SM00123G.

[4] Nerea Sebastián et al. "Electrooptics of mm-scale polar domains in the ferroelectric nematic phase". In: *Liquid Crystals* 48.14 (2021), pp. 2055–2071. DOI: 10.1080/02678292.2021.1955417. eprint: https://doi.org/10.1080/02678292.2021.1955417. URL: https://doi.org/10.1080/02678292.2021.1955417.

[5] Per Rudquist. "Revealing the polar nature of a ferroelectric nematic by means of circular alignment". In: *Scientific Reports* 11, 24411 (2021). DOI: 10.1038/s41598-021-04028-7. URL: https://www.nature.com/articles/s41598-021-04028-7.

[6] Pontus Jägemalm. *On the optics and surface physics of liquid crystals.* Doktorsavhandlingar vid Chalmers tekniska högskola: Ny serie 1512. Chalmers tekniska högsk., 1999. ISBN: 9171978119. URL: https://search.ebscohost.com/login.aspx?direct=true&db=cat09075a&AN=clpc.oai.edge.chalmers.folio.ebsco.com.fs00001000.5cfd5f51.8fac.489a.a146.d3327d64bee6&site=eds-live&scope=site&authtype=guest&custid=s3911979&groupid=main&profile=eds.

[7] Giovanni Barbero, Pontus Jägemalm, and Anatoly Zvezdin. "Temperature-induced surface transition in nematic liquid crystals oriented by evaporated SiO x". In: *Physical review. E, Statistical, nonlinear, and soft matter physics* 64 (Sept. 2001), p. 021703. DOI: 10.1103/PhysRevE.64.021703.

[8] John W. Goodby Peter J. Collings. *Introduction to Liquid Crystals, Chemistry and Physics, Second Edition.* Boca Raton: CRC Press, Oct. 2019. ISBN: 9781315098340. DOI: 10.1201/9781315098340.

[9] S. Chandrasekhar and D. Krishnamurti. “Birefringence of nematic liquid crystals”. In: *Physics Letters* 23.7 (1966), pp. 459–460. ISSN: 0031-9163. DOI: https://doi.org/10.1016/0031-9163(66)91094-8. URL: https://www.sciencedirect.com/science/article/pii/0031916366910948.

[10] Michael Allaby. *Michel–Lévy chart*. 2013. DOI: 10.1093/acref/9780199653065.013.5243. URL: https://www.oxfordreference.com/view/10.1093/acref/9780199653065.001.0001/acref-9780199653065-e-5243.

[11] Kohki Takatoh. *Alignment technologies and applications of liquid crystal devices*. The liquid crystals book series. Taylor & Francis, 2005. ISBN: 0748409025. URL: https://search.ebscohost.com/login.aspx?direct=true&db=cat09075a&AN=clpc.oai.edge.chalmers.folio.ebsco.com.fs00001000.981735e4.51b8.4d0e.9549.74b44c14489d&site=eds-live&scope=site&authtype=guest&custid=s3911979&groupid=main&profile=eds.

[12] John Janning. “Liquid crystal alignment structure”. US4165923A. Aug. 1979. URL: https://worldwide.espacenet.com/patent/search/family/026935248/publication/US4165923A?q=pn%5C%3DUS4165923A.

[13] Dana Ortansa Dorohoi et al. “Review on Optical Methods Used to Characterize the Linear Birefringence of Polymer Materials for Various Applications.” In: *Molecules* 28.7 (2023), p. 2955. ISSN: 14203049. URL: https://search.ebscohost.com/login.aspx?direct=true&db=edb&AN=163041941&site=eds-live&scope=site&authtype=guest&custid=s3911979&groupid=main&profile=eds.

[14] OLIVETTI & CO SPA. “TWISTED NEMATIC LIQUID CRYSTAL DISPLAY”. GB1446001A. Aug. 1976. URL: https://worldwide.espacenet.com/patent/search/family/023067746/publication/GB1446001A?q=pn%5C%3DGB1446001A.

[15] Stevie Brown et al. “Multiple Polar and Non-polar Nematic Phases”. In: *ChemPhysChem* 22.24 (2021), pp. 2506–2510. DOI: https://doi.org/10.1002/cphc.202100644. URL: https://chemistry-europe.onlinelibrary.wiley.com/doi/abs/10.1002/cphc.202100644.

[16] Max Born. “Über anisotrope Flüssigkeiten. Versuch einer Theorie der flüssigen Kristalle und des elektrischen Kerr-Effekts in Flüssigkeiten”. In: *Sitzungsber. Preuss. Akad Wiss* 30 (1916), pp. 614–650.

[17] Nerea Sebastián, Martin Čopič, and Alenka Mertelj. “Ferroelectric nematic liquid crystalline phases.” In: (2022). URL: https://search.ebscohost.com/login.aspx?direct=true&db=edsarx&AN=edsarx.2205.00193&site=eds-live&scope=site&authtype=guest&custid=s3911979&groupid=main&profile=eds.

[18] A.G. Khachaturyan. “Development of helical cholesteric structure in a nematic liquid crystal due to the dipole-dipole interaction”. In: *Journal of Physics and Chemistry of Solids* 36.10 (1975), pp. 1055–1061. ISSN: 0022-3697. DOI: https://doi.org/10.1016/0022-3697(75)90044-X. URL: https://www.sciencedirect.com/science/article/pii/002236977590044X.

[19] A.M.J. Spruijt. “The twist-disclination line in planar oriented samples of liquid crystals”. In: *Solid State Communications* 13.11 (1973), pp. 1919–1922. ISSN: 0038-1098. DOI: https://doi.org/10.1016/0038-1098(73)90758-8. URL: https://www.sciencedirect.com/science/article/pii/0038109873907588.

A

Predictions

This appendix contains a number of predictions of the configuration of $\hat{\mathbf{n}}$ in an ECRC at a number of different values of ϕ. To create the predictions, the following has been assumed:

- The absolute value of ϕ is constant across the whole evaporated surface.
- In the N phase, the sign of ϕ is chosen such that the twist deformation required to satisfy the BCs is minimized.
- In version A the N_F phase, the sign of ϕ is chosen such that the twist deformation required to satisfy the BCs is minimized.
- In version B of the N_F phase, the sign of ϕ remains the same as in the N phase.
- The energy required to form disclinations and domain borders is ignored.

In the images, the evaporation direction is marked by a dashed arrow, and always points to the right. The black circle shows the direction of the circular rubbing. The black lines and arrows represent the alignment of $\hat{\mathbf{n}}$ at the circularly rubbed surface, and the red lines and arrows represent its alignment on the evaporated surface. The dashed lines show borders between domains where ϕ has different signs, which may or may not coincide with twist disclinations. The dotted lines represent pure twist disclinations. At edges between red and green fields without a dashed or dotted lines, the LC is non-twisted.

The predictions for version A of the N_F phase alignment are not consistent with what is seen experimentally. Version B, however, seem to agree with the results in this thesis. The difference is that the borders going from left to right tend to point slightly downwards in real ECRCs, and that the twist disclinations do not appear in all cells. This differences may be due to pretilt, or due to the spontaneous twist predicted by Kachaturyan [18].

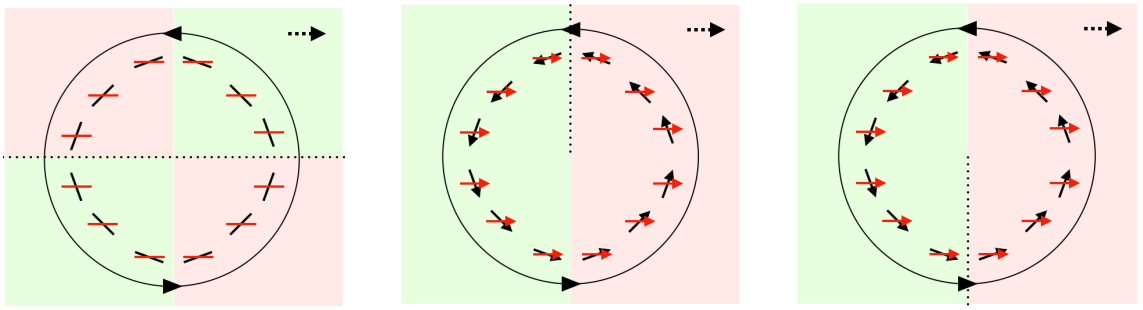

(a) N **(b)** N_F, version A **(c)** N_F, version B

Figure A.1: $\phi = 0°$

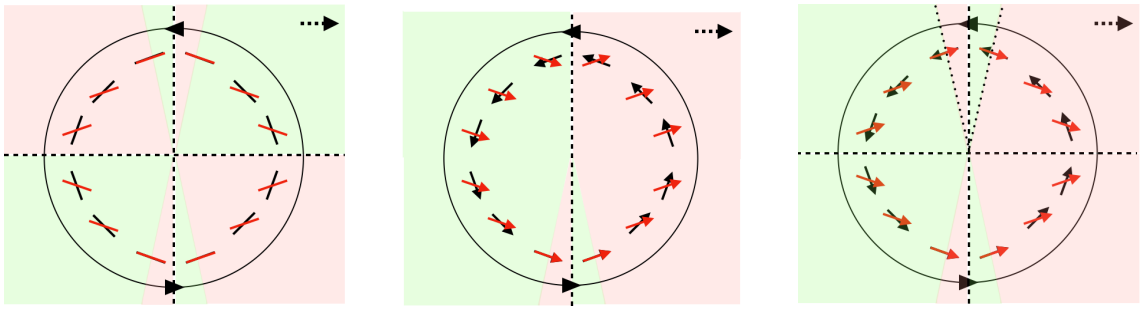

(a) N **(b)** N_F, version A **(c)** N_F, version B

Figure A.2: $\phi = 19°$

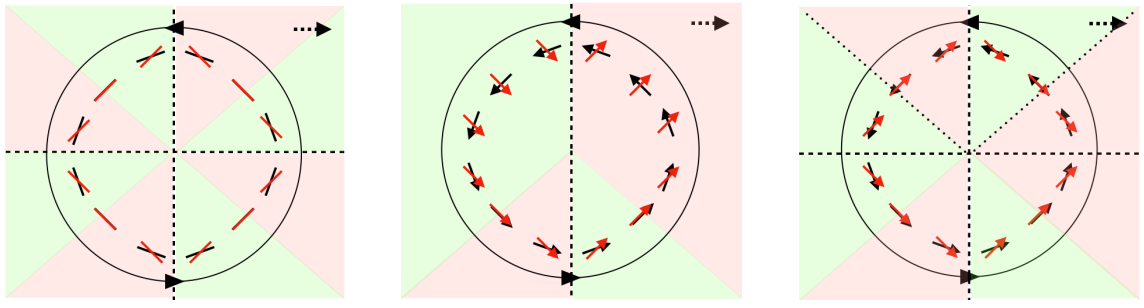

(a) N **(b)** N_F, version A **(c)** N_F, version B

Figure A.3: $\phi = 45°$

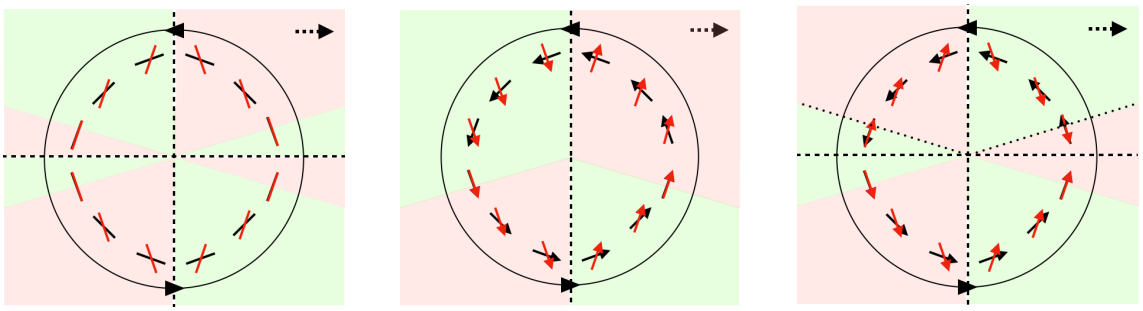

(a) N **(b)** N_F, version A **(c)** N_F, version B

Figure A.4: $\phi = 71°$

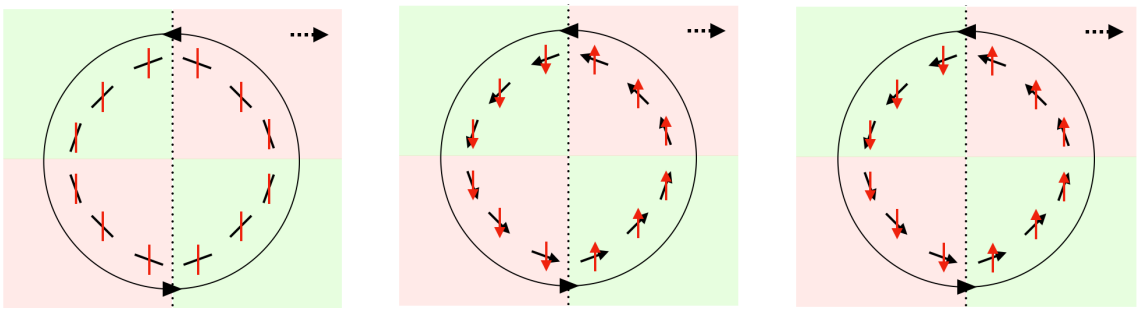

(a) N **(b)** N_F, version A **(c)** N_F, version B

Figure A.5: $\phi = 90°$

DEPARTMENT OF MICROTECHNOLOGY AND NANOSCIENCE
CHALMERS UNIVERSITY OF TECHNOLOGY
Gothenburg, Sweden
www.chalmers.se

CHALMERS
UNIVERSITY OF TECHNOLOGY